ARTICLE IN PRESS

Robotics and Autonomous Systems ▮ (▮▮▮▮) ▮▮▮–▮▮▮

Contents lists available at ScienceDirect

Robotics and Autonomous Systems

journal homepage: www.elsevier.com/locate/robot

Integral admittance shaping: A unified framework for active exoskeleton control

Umashankar Nagarajan [a], Gabriel Aguirre-Ollinger [b,*], Ambarish Goswami [c]

[a] Google Inc., Mountain View, CA 94043, United States

[b] Centre for Autonomous Systems, University of Technology, Sydney, Broadway, NSW 2007, Australia

[c] Honda Research Institute, USA, Mountain View, CA 94043, United States

HIGHLIGHTS

- A control method for lower-limb exoskeletons based on modifying the dynamic response of the legs.
- Active control renders the lower limbs more responsive to muscle torques generated by the human.
- Optimization method synthesizes a controller capable of generating the desired dynamic response.
- Optimization also ensures the stability and passivity of the coupled human limb exoskeleton.
- Control robustness to parameter uncertainties is analyzed and discussed.

ARTICLE INFO

Article history:
Received 6 April 2015
Received in revised form
3 September 2015
Accepted 12 September 2015
Available online xxxx

Keywords:
Exoskeleton control
Powered exoskeletons
Assistive robotics
Wearable robots
Admittance control
Rehabilitation

ABSTRACT

Current strategies for lower-limb exoskeleton control include motion intent estimation, which is subject to inaccuracies in muscle torque estimation as well as modeling error. Approaches that rely on the phases of a uniform gait cycle have proven effective, but lack flexibility to aid other kinds of movement. This research aims at developing a more versatile control that can assist the lower limbs independently of the movement attempted. Our control strategy is based on modifying the dynamic response of the human limbs, specifically their mechanical admittance. Increasing the admittance makes the lower limbs more responsive to any muscle torque generated by the human user.

We present *Integral Admittance Shaping*, a unified mathematical framework for: (a) determining the desired dynamic response of the coupled system formed by the human limb and the exoskeleton, and (b) synthesizing an exoskeleton controller capable of achieving said response.

The present control formulation focuses on single degree-of-freedom exoskeleton devices providing performance augmentation. The algorithm generates a desired shape for the frequency response magnitude of the integral admittance (torque-to-angle relationship) of the coupled system. Simultaneously, it generates an optimal feedback controller capable of achieving the desired response while guaranteeing coupled stability and passivity. The potential effects of the exoskeleton's assistance are motion amplification for the same joint torque, and torque reduction for the same joint motion. The robustness of the derived exoskeleton controllers to parameter uncertainties is analyzed and discussed. Results from initial trials using the controller on an experimental exoskeleton are presented as well.

1. Introduction

The last two decades have seen the development of a large number of exoskeleton devices aimed at assisting humans in their physical activities. Lower-limb exoskeleton systems have been designed for rehabilitation [1,2], load carrying [3,4], and performance augmentation [5,6]. Other systems include upper-body exoskeletons for movement assistance [7–9], rehabilitation [10,11] and haptic interaction [12,13], as well as a number of whole-body assistive devices [5,14].

1.1. Assistive strategies for human locomotion

The focus of the present study is lower-limb exoskeleton control. The following is an overview of some of the most common

* Corresponding author.
E-mail addresses: umashankarn@google.com (U. Nagarajan), gabriel.aguirre-ollinger@uts.edu.au (G. Aguirre-Ollinger), agoswami@hra.com (A. Goswami).

http://dx.doi.org/10.1016/j.robot.2015.09.015
0921-8890/

Please cite this article in press as: U. Nagarajan, et al., Integral admittance shaping: A unified framework for active exoskeleton control, Robotics and Autonomous Systems (2015), http://dx.doi.org/10.1016/j.robot.2015.09.015

strategies for assisting human locomotion by means of an exoskeleton.

- *Muscle effort reduction*. This category includes devices that aim at reducing the muscle effort needed for human locomotion at a given speed. In [15], electromyographic (EMG) feedback control provided torque assist to the hip, knee and ankle joints during locomotion. The system reported in [16] demonstrated experimentally that, while walking at a given speed, humans learn to reduce their muscle activations when appropriate assistive torques are added to their ankle joints. In [17], it was demonstrated that providing assistance at the hip joint can reduce muscle activations at both the hip and ankle joints during walking.
- *Metabolic cost reduction*. A number of studies have demonstrated reduction in metabolic cost when walking in a tethered exoskeleton, i.e. one with an off-board power supply [18–20]. An assistive device with on-board power and actuation that experimentally demonstrated reduction in metabolic cost during load carriage was reported in [21]. For activities like hopping, which involve spring-like behavior, researchers have demonstrated reduction in metabolic cost by adding passive elements in parallel with the human joints [22,23]. Several control strategies were tested in [24] with a knee exoskeleton, which experimentally demonstrated reduction in energy expenditure during squatting.
- *Walking speed increase*. Increase in walking speed for a given muscle effort could be achieved by an exoskeleton that contributes to increase either stride length or stepping frequency. Powered ankle–foot orthoses were used in [25] to demonstrate that the preferred walking speed of humans can potentially be increased by providing assistive torques at the ankle joints. In [26], a pneumatic-muscle exoskeleton enabled increase in step length while keeping the step frequency constant. It was demonstrated in [27] that the natural frequency of the leg around the knee joint can be modified using impedance control. Active admittance control was used to experimentally demonstrate increase in natural frequency of leg swing at the knee joint [28].

Every assistive strategy requires in turn an appropriate exoskeleton control. Current control methods include EMG feedback [29,15], linking exoskeleton torques to the phases of the gait cycle [30,20,31,17], facilitating a clinically correct gait via soft constraints [32] and modifying the dynamic response of the lower limbs by means of active admittance [33] or generalized elasticities [34]. Additionally, the view of human gait as a stable limit cycle has led to the emergence of oscillator-based controls [35–37].

1.2. A task-independent control strategy

Most of the control methods described above have strengths but also limitations. For example, intent estimation is conditioned by the respective accuracies of the muscle torque estimates and the human musculoskeletal model. Systems that time the assistive torques to the phases of the gait cycle are often limited to assisting uniform-speed gait. Our research is motivated by the desire for a more versatile control, namely, one that is capable of assisting the lower limbs independently of the motion task attempted.

This paper presents a mathematical framework for exoskeleton control based on the idea of producing a desired dynamic response in the leg by coupling it to the exoskeleton. Here, dynamic response is understood as the relationship between the net muscle torque exerted on a human joint, and the resulting angular motion of the joint. Our approach pursues two main objectives: (a) specifying the exoskeleton's assistive action in terms of a desired dynamic response, and (b) designing an exoskeleton controller capable of producing the desired response. The work presented here focuses on single-joint motion and uses linearized models of the exoskeleton and the human limb. Examples of lower-limb exoskeletons assisting a single joint include Honda's Stride Management Assist (SMA) device [38], Yobotics' RoboKnee device [6] and Yaskawa's Ankle-Assist device [39].

Our control scheme assists lower-limb movement in an indirect way by producing a virtual increase in the amplitude of the leg's dynamic response. This increase is not caused by a change in the properties of the leg's musculoskeletal system, but results from coupling the leg to an exoskeleton endowed with active dynamics. The leg's desired dynamic response is defined by the magnitude profile of its frequency response function. More precisely, we specify the *integral admittance*, i.e. the muscle torque to joint angle relationship of the assisted leg. We use integral admittance rather than admittance in order to control the leg's response at zero frequency as well. Thus, we refer to our mathematical framework as *integral admittance shaping*. The associated control problem consists of obtaining the optimal control parameters that will produce the desired frequency response in the coupled system formed by the human limb and the exoskeleton (henceforth referred to as the *coupled human–exoskeleton system*). In this scheme, assistance can take two possible forms: motion amplification, i.e., larger motion amplitude for the same muscle torque, or torque reduction, i.e., reduction in the torque amplitude required to achieve the same motion amplitude.

In order to make the integral admittance of the coupled human–exoskeleton system larger than that of the unassisted limb, the exoskeleton controller first needs to overcome its own impedance, and then partially compensate the impedance of the human joint. This requires the exoskeleton to display active behavior, which in turn requires ensuring the stability of the coupled system. Furthermore, the stability of the coupled system needs to be guaranteed when the leg is in contact with external environments [40], for example during foot contact with the ground. This requires a stronger condition than simple stability: the coupled system must be *passive* as well [41]. Passivity in this context refers to the transfer function relating net muscle torque to the angular motion of the human limb coupled to the exoskeleton. Our integral admittance shaping framework generates exoskeleton controls capable of ensuring both the stability and passivity of the assisted limb.

The optimization method presented here is complemented with an analysis of the robust stability, passivity and performance margins of assistive controllers designed using the integral admittance shaping framework in the presence of parameter uncertainties. Finally, we present results from an initial trial involving subjects walking in a modified version of the Stride Management Assist (SMA), an autonomous powered exoskeleton developed by Honda Motor Co., Ltd. (Fig. 1). This paper is an extended version of a previous conference submission [42].

2. Joint dynamics of a coupled human–exoskeleton system

The mathematical framework presented in this paper uses an elementary model that consists of linearized 1-DOF models for the human leg and the exoskeleton. The 1-DOF leg model is an approximation of the extended leg swinging about the hip joint. Although simple, this model is useful to capture the swing phase of the gait cycle and other unconstrained motions of the leg. Accordingly, the control developed here is primarily intended for devices that assist hip joint motion, such as the experimental exoskeleton of Fig. 1.

In modeling the system, we have to consider the compliance of the physical coupling between the exoskeleton and the human

Please cite this article in press as: U. Nagarajan, et al., Integral admittance shaping: A unified framework for active exoskeleton control, Robotics and Autonomous Systems (2015), http://dx.doi.org/10.1016/j.robot.2015.09.015

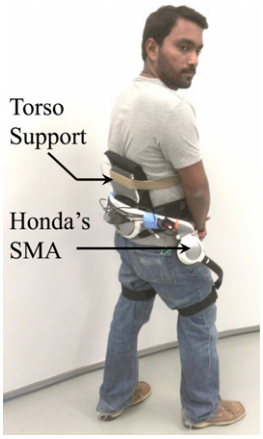

Fig. 1. A human subject wearing an experimental exoskeleton with actuators to assist hip-joint motion. The device features a back support to increase the rigidity of the coupling with the human torso.

limb (Fig. 2). Coupling compliance has an important effect on the coupled system's stability in the presence of feedback control.

The linear equations of motion of the coupled human–exoskeleton system with compliant coupling are given by

$$I_h\ddot{\theta}_h(t) + b_h\dot{\theta}_h(t) + k_h\theta_h(t) = \tau_h(t) - \tau_c(t), \tag{1}$$

$$I_e\ddot{\theta}_e(t) + b_e\dot{\theta}_e(t) + k_e\theta_e(t) = \tau_e(t) + \tau_c(t). \tag{2}$$

The terms in (1) and (2) are described as follows:

- I_h, b_h, k_h are, respectively, the moment of inertia, joint damping coefficient and joint stiffness coefficient of the human leg; $\theta_h(t)$ is the hip joint angle trajectory and $\tau_h(t)$ is the net muscle torque acting on the joint. The term $k_h\theta_h(t)$ includes the linearized gravitational torque.
- I_e, b_e, k_e are, respectively, the moment of inertia, joint damping coefficient and joint stiffness coefficient of the exoskeleton; $\theta_e(t)$ is exoskeleton arm's angle trajectory and $\tau_e(t)$ is the actuator torque.
- τ_c is the coupling torque representing the interaction between exoskeleton and the human limb.

Coupling compliance is the combined effect of the intervening human tissues and the exoskeleton's attachment devices. We model the soft coupling by an equivalent linear spring and damper combination with stiffness coefficient k_c and damping coefficient b_c. Therefore the coupling torque in (1) and (2) is given by

$$\tau_c(t) = b_c(\dot{\theta}_h(t) - \dot{\theta}_e(t)) + k_c(\theta_h(t) - \theta_e(t)). \tag{3}$$

2.1. Shaping the leg dynamics via impedance perturbations

Our approach to lower-limb assistance is based of modifying the dynamic response of the leg, specifically the relationship between the net muscle torque exerted on the leg and the resulting angular motion. Thus we model the ideal effect of assisting the human limb as applying an additive perturbation δZ_h to the limb's natural impedance Z_h. The perturbed impedance is then

$$\widetilde{Z}_h = Z_h + \delta Z_h. \tag{4}$$

An equivalent expression can be given in terms of the leg's admittance, $Y_h(s) = Z_h(s)^{-1}$. The perturbed admittance of the leg, $\widetilde{Y}_h(s)$, is represented by a negative feedback system formed by Y_h and δZ_h:

$$\widetilde{Y}_h = \frac{1}{Z_h + \delta Z_h} = \frac{Y_h}{1 + Y_h\delta Z_h}. \tag{5}$$

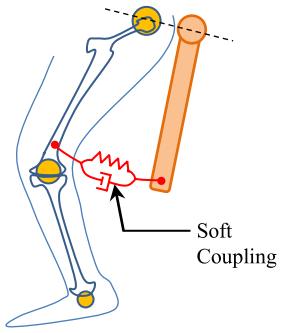

Fig. 2. A simple human limb and exoskeleton model with compliant coupling between the human limb and the exoskeleton arm.

In our scheme, assistance happens when $\widetilde{Y}_h$ is such that the subject can move the leg with more ease than in the unassisted case, represented by the leg's normal admittance Y_h. In (5), the perturbed admittance is represented as the coupling of two dynamical systems: the leg's original admittance Y_h, and the impedance perturbation δZ_h. Given that we intend to assist by coupling the lower limbs to an exoskeleton, (5) suggests a simple design strategy: substitute δZ_h with the exoskeleton's impedance, $Z_e(s)$, and design an exoskeleton control capable of modifying $Z_e(s)$. The control design objective is to generate $Z_e(s)$ such that the coupled leg–exoskeleton system emulates the behavior of $\widetilde{Y}_h$ as closely as possible.

2.2. Integral admittance

We now discuss briefly the models of the human limb, the exoskeleton and the coupling between the two. For the linear human joint dynamics in (1), the admittance transfer function $Y_h(s)$ is given by

$$Y_h(s) = \frac{\Omega_h(s)}{\tau_h(s)} = \frac{s}{I_h s^2 + b_h s + k_h}, \tag{6}$$

where $\Omega_h(s)$ is the Laplace transform of the angular velocity $\dot{\theta}_h(t)$, and $\tau_h(s)$ is the Laplace transform of the muscle torque $\tau_h(t)$.

For the purposes of control design, however, we shall focus on the integral of the admittance, $Y_h(s)/s$, which relates the net muscle torque to the angular position of the leg. We use this rather than the leg's admittance in order to consider the effects of the exoskeleton at low frequencies, as well as the "DC gain" (zero-frequency response) of the leg. Thus we define the *integral admittance* transfer function $X_h(s)$ as

$$X_h(s) = \frac{\Theta_h(s)}{\tau_h(s)} = \frac{Y_h(s)}{s}. \tag{7}$$

The admittance transfer function of the exoskeleton, $Y_e(s)$, is given by

$$Y_e(s) = \frac{\Omega_e(s)}{\tau_e(s)} = \frac{s}{I_e s^2 + b_e s + k_e}. \tag{8}$$

The impedance transfer function $Z_c(s)$ of the coupling element between the leg and the exoskeleton, derived from (3), is given by

$$Z_c(s) = \frac{\tau_c(s)}{\Omega_c(s)} = \frac{b_c s + k_c}{s}, \tag{9}$$

where $\Omega_c(s) = \Omega_h(s) - \Omega_e(s)$.

2.3. Closed-loop coupled human–exoskeleton system

This section derives the closed-loop dynamics of the coupled human–exoskeleton system with feedback control, and formulates its coupled stability and passivity conditions. The coupled

Please cite this article in press as: U. Nagarajan, et al., Integral admittance shaping: A unified framework for active exoskeleton control, Robotics and Autonomous Systems (2015), http://dx.doi.org/10.1016/j.robot.2015.09.015

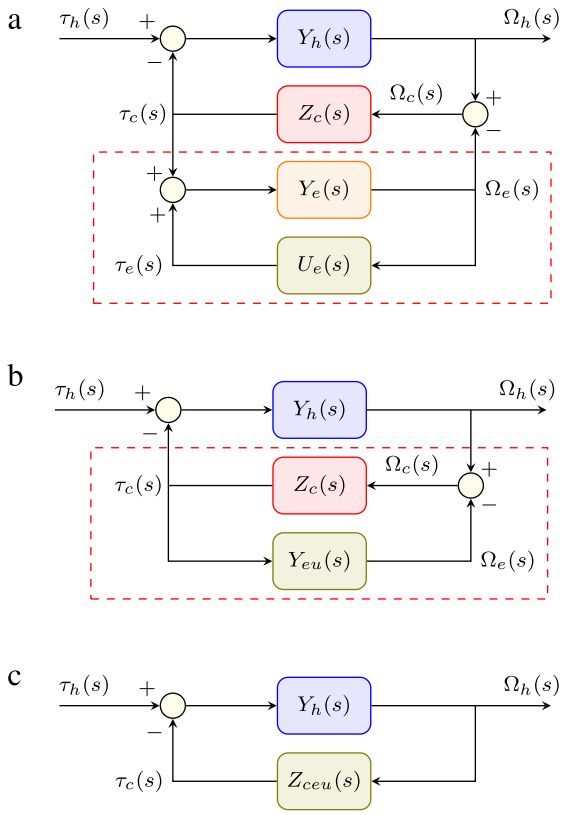

Fig. 3. Block diagram of the coupled human–exoskeleton system with exoskeleton control. The controller $U_e(s)$ and unpowered exoskeleton admittance $Y_e(s)$ in (a) are combined to form $Y_{eu}(s)$ in (b) using (10). $Y_{eu}(s)$ and the isolated coupling impedance $Z_c(s)$ in (b) are combined to form $Z_{ceu}(s)$ in (c) using (11). The stability of the coupled system is determined from the open-loop transfer function $L_{ceu}(s) = Y_h(s)Z_{ceu}(s)$.

human–exoskeleton system (1)–(3) is represented by the block diagram of Fig. 3(a). The exoskeleton control consists of a feedback compensator $U_e(s)$ that takes the angular velocity $\Omega_e(s)$ of the exoskeleton arm as input, and generates an actuator torque $\tau_e(s)$. Because the exoskeleton has to display active behavior, i.e. source energy to the leg, positive feedback is assumed.

When the compensator $U_e(s)$ is active, the exoskeleton passive dynamics $Y_e(s)$ are replaced by the closed-loop system outlined region in Fig. 3(a), which can be reduced to a single transfer function $Y_{eu}(s)$ given by

$$Y_{eu}(s) = \frac{Y_e(s)}{1 - Y_e(s)U_e(s)}, \tag{10}$$

as shown in Fig. 3(b).

Similarly, the outlined region containing $Z_c(s)$ and $Y_{eu}(s)$ in Fig. 3(b) can be reduced to a single transfer function $Z_{ceu}(s)$ given by

$$Z_{ceu}(s) = \frac{Z_c(s)}{1 + Z_c(s)Y_{eu}(s)}, \tag{11}$$

as shown in Fig. 3(c).

$Z_{ceu}(s)$ represents the external dynamical system acting on the leg; it is composed of the passive dynamics of the exoskeleton mechanism, the feedback compensator, and the dynamics of the compliant coupling joining the leg and exoskeleton arm. From Fig. 3(c), the closed-loop admittance $Y_{heu}(s)$ of the coupled human–exoskeleton system (with the exoskeleton controller $U_e(s)$ in place) is given by

$$Y_{heu}(s) = \frac{\Omega_h(s)}{\tau_h(s)} = \frac{Y_h(s)}{1 + Y_h(s)Z_{ceu}(s)}. \tag{12}$$

The corresponding closed-loop integral admittance $X_{heu}(s)$ is given by

$$X_{heu}(s) = \frac{Y_{heu}(s)}{s} = \frac{\Theta_h(s)}{\tau_h(s)} = \frac{X_h(s)}{1 + Y_h(s)Z_{ceu}(s)}. \tag{13}$$

$X_{heu}(s)$ represents the dynamic response of the leg when coupled the exoskeleton. Assistance can now be formulated in precise terms as a desired frequency response profile for $X_{heu}(j\omega)$. The control problem then consists of designing a compensator $U_e(s)$ capable of producing the desired shape of $X_{heu}(j\omega)$.

In order to design the exoskeleton control, it is essential to ensure the stability of the coupled system formed by the $Y_h(s)$ and $Z_{ceu}(s)$ (Fig. 3(c)). Stability can be determined from the gain margin of the system's loop transfer function $L_{heu}(s)$, given by

$$L_{heu}(s) = Y_h(s)Z_{ceu}(s). \tag{14}$$

Since the closed-loop system has a positive feedback loop, one needs to look at the gain margin of $-L_{heu}(s)$ to evaluate its stability. The gain margin is given by

$$GM(L_{heu}) = \frac{1}{|L_{heu}(j\omega_c)|}, \tag{15}$$

where ω_c is the phase-crossover frequency, i.e. the frequency for which $\angle -L_{heu}(j\omega_c) = 180°$. In order for the coupled human–exoskeleton system to be stable, the following condition needs to be satisfied:

$$GM(L_{heu}) > 1. \tag{16}$$

For dynamically interacting systems, a stronger requisite than coupled stability is coupled passivity, which ensures that the coupled human–exoskeleton system does not become unstable when in contact with any passive environment [40], for example when the foot contacts the ground. Therefore, a specific objective in our control design is to ensure that the transfer function $X_{heu}(s)$ is passive as well. Based on [41] it can be shown that, for the coupled human–exoskeleton system (16) to be passive, the following phase condition must be satisfied:

$$\angle X_{heu}(j\omega) \in [-180°, 0°] \quad \forall\omega. \tag{17}$$

3. Integral admittance shaping

This section formally presents *integral admittance shaping*, a unified mathematical framework for (a) determining the desired dynamic response of the coupled human–exoskeleton system, and (b) synthesizing an exoskeleton controller capable of achieving the desired response.

We begin by providing conceptual and quantitative definitions of assistance and resistance in terms of the frequency response of the integral admittance. These definitions are then employed to make a quantitative formulation of the desired dynamic properties of the human–exoskeleton system; this formulation includes goals of performance as well as stability and passivity. Finally, a constrained optimization generates the necessary parameter values for the exoskeleton control.

3.1. Assistance and resistance

If we consider the case of the leg moving without ground contact, for example during the swing phase of walking, there are two ways in which the leg can be said to be assisted. One is when, for a given muscle torque amplitude, the amplitude of the leg's angular motion is larger than in the unassisted case. We refer to this effect as *motion amplification*. The other one is when, for a given angular motion amplitude, the required muscle torque amplitude

Please cite this article in press as: U. Nagarajan, et al., Integral admittance shaping: A unified framework for active exoskeleton control, Robotics and Autonomous Systems (2015), http://dx.doi.org/10.1016/j.robot.2015.09.015

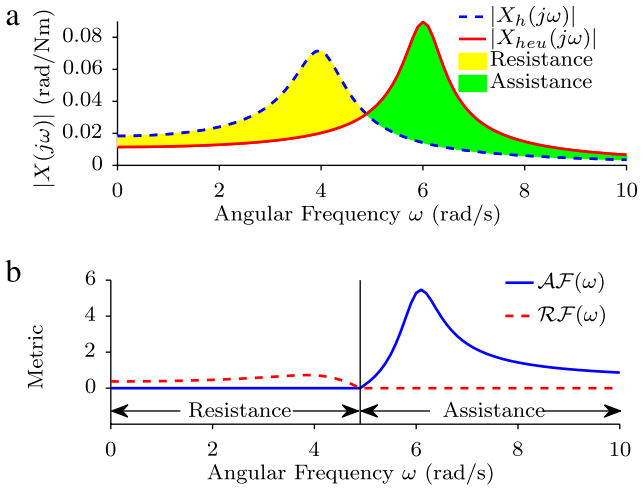

Fig. 4. Assistance and resistance in a hypothetical linear model of the human limb coupled to an exoskeleton. The isolated human leg is represented by the integral admittance $|X_h(j\omega)|$; the coupled human exoskeleton system has integral admittance $|X_{heu}(j\omega)|$. (a) Frequency response plots show that, for the coupled system, there can be simultaneously a frequency range in which the muscles are subject to assistance ($|X_{heu}(j\omega)| > |X_h(j\omega)|$), and a frequency range in which the muscles are subject to resistance ($|X_{heu}(j\omega)| < |X_h(j\omega)|$). Said ranges are mutually exclusive. In this example, resistance occurs at lower frequencies, and assistance at higher frequencies. (b) The respective levels of assistance and resistance are quantified by two metrics, the assistance function $\mathcal{AF}(\omega)$ (19), and the resistance function $\mathcal{RF}(\omega)$ (21). (For interpretation of the references to color in this figure legend, the reader is referred to the web version of this article.)

is smaller than in the unassisted case. We call this second effect *torque reduction*. What these two effects have in common is that they can be modeled as an increase in the magnitude of leg's integral admittance. Clearly, the admittance properties of the physical leg itself do not change. But, as Eq. (13) suggests, it is possible to produce a *virtual change* in the leg's integral admittance by coupling it to an exoskeleton displaying an appropriate impedance.

$X_h(s)$ and $X_{heu}(s)$ are, respectively, the integral admittance of the isolated human leg and the integral admittance of the coupled human–exoskeleton system. Because $X_{heu}(s)$ controls the relationship between muscle torque and leg angle when the exoskeleton is attached, we can think of $X_{heu}(s)$ as the integral admittance of the assisted leg. This in turn allows us to formulate a concise definition of assistance:

Definition 1. A 1-DOF human limb joint is said to be *assisted* by an exoskeleton if the magnitude of the integral admittance of the coupled limb–exoskeleton system is greater than that of the free limb, for all frequencies of interest.

Thus when the leg moves at a certain frequency ω, the hip joint is assisted by the exoskeleton when $|X_{heu}(j\omega)| > |X_h(j\omega)|$, and it is resisted when $|X_{heu}(j\omega)| < |X_h(j\omega)|$. This comparison is valid because both transfer functions relate the same variables, namely the net muscle torque $\tau_h(s)$, to the leg angle $\Theta(s)$.

Fig. 4(a) shows the frequency response magnitude profiles of an unassisted human leg and a hypothetical coupled human–exoskeleton system. (Differences between the two frequency responses are exaggerated for the purposes of illustration.) Per Definition 1, the green-colored region corresponds to the frequencies where the human limb undergoes *assistance*, i.e., $|X_{heu}(j\omega)| > |X_h(j\omega)|$, and the yellow-colored one to frequencies where the leg undergoes *resistance*, i.e., $|X_{heu}(j\omega)| < |X_h(j\omega)|$. From Fig. 4 it can be seen that the frequency ranges for assistance and resistance are mutually exclusive.

Using the preceding definitions, we propose the following quantitative metric for assistance:

Definition 2. *Assistance Ratio* $\mathcal{A}(\omega_f)$ is defined as the mean increase in admittance over a range of possible motion frequencies $[0, \omega_f]$, and is given by

$$\mathcal{A}(\omega_f) = \frac{1}{\omega_f}\int_0^{\omega_f} \mathcal{AF}(\omega)d\omega \tag{18}$$

where the assistance function $\mathcal{AF}(\omega)$ is given by

$$\mathcal{AF}(\omega) = \max\left(\frac{|X_{heu}(j\omega)| - |X_h(j\omega)|}{|X_h(j\omega)|},\ 0\right). \tag{19}$$

The interpretation of this assistance metric is as follows. $\mathcal{AF}(\omega)$ represents the fraction by which the leg's admittance increases at a given frequency ω. (Where the admittance decreases, $\mathcal{AF}(\omega)$ evaluates to zero.) Thus, assuming the leg can move with any frequency up to ω_f, $\mathcal{A}(\omega_f)$ represents the mean increase in admittance over $[0, \omega_f]$.

The quantitative metric for resistance is defined in an entirely analogous manner:

Definition 3. *Resistance Ratio* $\mathcal{R}(\omega_f)$ is defined as the mean decrease in admittance over the same range of frequencies $[0, \omega_f]$, and is given by

$$\mathcal{R}(\omega_f) = \frac{1}{\omega_f}\int_0^{\omega_f} \mathcal{RF}(\omega)d\omega \tag{20}$$

where the resistance function $\mathcal{RF}(\omega)$ is given by

$$\mathcal{RF}(\omega) = \min\left(\frac{|X_h(j\omega)| - |X_{heu}(j\omega)|}{|X_h(j\omega)|},\ 0\right). \tag{21}$$

A key point about these metrics is that, for a frequency range $[0, \omega_f]$, it is possible (although not necessary) to have both $\mathcal{A}(\omega_f) > 0$ and $\mathcal{R}(\omega_f) > 0$. This is so because, as Fig. 4 shows, assistance and resistance occur at mutually exclusive frequencies. Using these metrics, the following section enumerates the desired characteristics of a coupled human–exoskeleton system involving assistance.

3.2. Desired characteristics of an assisted coupled human–exoskeleton system

Our present aim is for the exoskeleton control to produce assistance over a certain range of frequencies and no resistance over the remaining frequencies. Simultaneously, we need to ensure that the coupled human–exoskeleton system is both stable and passive. Therefore, the desired characteristics of the assisted 1-DOF coupled human–exoskeleton system are listed as follows:

- coupled stability: $GM(L_{heu}) > 1$ (Eq. (16));
- coupled passivity: $\angle X_{heu}(j\omega) \in [-180°, 0°], \forall\omega$ (Eq. (17));
- positive assistance: $\mathcal{A}(\omega_f) > 0$ (Eq. (18)); and
- no resistance: $\mathcal{R}(\omega_f) = 0$ (Eq. (20)).

It must be noted that passivity of the coupled human–exoskeleton system does not imply by any means that the controlled exoskeleton itself should be passive. As we will show in the next section, the isolated exoskeleton has to exhibit active behavior in order to provide any net assistance.

Comfort is an additional performance characteristic to consider. Since the human's sensorimotor control is attuned to the leg's damping ratio ζ_h, we theorize that, if the exoskeleton produces an excessive variation in damping ratio, this can lead to user discomfort. For example, if the damping ratio ζ_{heu} of the coupled system is significantly lower than that of the unassisted leg, then the coupled system will exhibit a stronger tendency to oscillate,

Please cite this article in press as: U. Nagarajan, et al., Integral admittance shaping: A unified framework for active exoskeleton control, Robotics and Autonomous Systems (2015), http://dx.doi.org/10.1016/j.robot.2015.09.015

which might be difficult for the user to control. Conversely, an excessively large damping ratio may cause the limb to feel sluggish. Therefore, as an additional constraint, we limit the allowable damping ratio variation:

$$\frac{|\zeta_{heu} - \zeta_h|}{\zeta_h} < \epsilon, \tag{22}$$

where ϵ is the allowed variation in the damping ratio of the human joint.

3.3. Exoskeleton control law

Now that we have the necessary metrics for assistance, we proceed to shape the closed-loop integral admittance of the human–exoskeleton system based on these metrics. To this end, we need to derive an appropriate exoskeleton controller $U_e(s)$. If we specify the desired exoskeleton dynamics by a moment of inertia I_e^d, joint damping coefficient b_e^d and joint stiffness coefficient k_e^d, then an intuitive control law would be

$$U_e(s) = K_\alpha s + K_\omega + \frac{K_\theta}{s}, \tag{23}$$

where the control gains are given by

$$\begin{aligned} K_\alpha &= I_e - I_e^d \\ K_\omega &= b_e - b_e^d \\ K_\theta &= k_e - k_e^d. \end{aligned} \tag{24}$$

This reduces the isolated exoskeleton dynamics in (2) to

$$I_e^d \ddot{\theta}_e(t) + b_e^d \dot{\theta}_e(t) + k_e^d \theta_e(t) = 0. \tag{25}$$

Per our definition of assistance, the exoskeleton needs to cancel its own impedance and compensate the human leg's impedance. This requires making $k_e^d < 0$ to compensate for the human joint stiffness (as well as the gravitational torque), $b_e^d < 0$ to compensate for the human joint damping, and $I_e^d < 0$ to compensate for the human limb's moment of inertia, thereby making the gains (24) positive. In other words, the controller uses *positive feedback* in order to achieve the desired exoskeleton dynamics (25).

A natural question is whether it is possible to maintain the stability of the coupled exoskeleton–human system when positive feedback is involved. In previous work [43,44], we have shown that stiffness compensation ($K_\theta > 0$) and damping compensation ($K_\omega > 0$) are relatively straightforward to implement; the stability of the coupled system is maintained due to the passive impedance of the human limb. By contrast, inertia compensation ($K_\alpha > 0$) is a non-trivial problem. Appendix B shows how, with unfiltered positive acceleration feedback, the controller can at most cancel the exoskeleton inertia I_e, but not compensate any fraction of the human limb inertia I_h, before the coupled system becomes unstable.

Interestingly, low-pass filtering the acceleration signal overcomes this limitation [28]. In Appendix C, we show how a low-pass filter allows placing the dominant poles of the coupled system at locations consistent with a virtual reduction in the human limb inertia. Therefore, we propose the following control law for the exoskeleton:

$$U_e(s) = K_\alpha H_{lo}(s) s + K_\omega + \frac{K_\theta}{s}, \tag{26}$$

where $H_{lo}(s)$ is a low-pass filter for the measured angular acceleration. Based on the results from Appendix C, we select a second-order low-pass Butterworth filter given by

$$H_{lo}(s) = \frac{\omega_{lo}^2}{s^2 + \sqrt{2}\omega_{lo} s + \omega_{lo}^2}, \tag{27}$$

where ω_{lo} is the cut-off frequency.

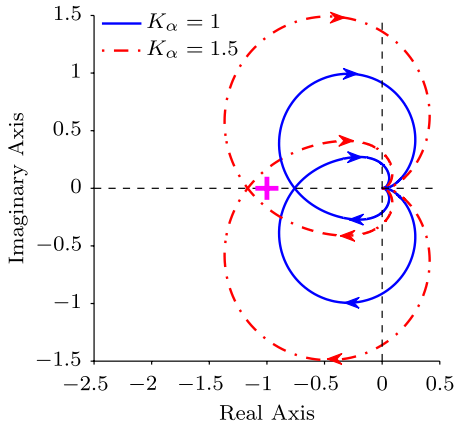

Fig. 5. Nyquist plots of $L_{heu}(s)$ with the exoskeleton controller $U_e(s)$ in (26) for $K_\alpha = 1$ and $K_\alpha = 1.5$ kg m^2, with the other control parameters fixed at $K_\theta = K_\omega = 0$ and $\omega_{lo} = 10$ rad/s. Since $L_{heu}(s)$ has no unstable poles, the number of encirclements of the Nyquist plot around -1 is sufficient to determine the stability of the closed-loop system. For $K_\alpha = 1$ kg m^2, its Nyquist plot does not encircle -1 resulting in a stable closed-loop system, whereas for $K_\alpha = 1.5$ kg m^2, its Nyquist plot encircles -1 twice resulting in an unstable closed-loop system.

Fig. 5 shows the Nyquist plots of $L_{heu}(s)$ with the exoskeleton controller $U_e(s)$ in (26) for $K_\alpha = 1$ and $K_\alpha = 1.5$ kg m^2, while the remaining control parameters were fixed at $K_\theta = K_\omega = 0$ and $\omega_{lo} = 10$ rad/s. Since $L_{heu}(s)$ has no unstable poles, the number of encirclements of the Nyquist plot around -1 is sufficient to determine the stability of the closed-loop system. For $K_\alpha = 1$ kg m^2, its Nyquist plot does not encircle -1 resulting in a stable closed-loop system, whereas for $K_\alpha = 1.5$ kg m^2, its Nyquist plot encircles -1 twice resulting in an unstable closed-loop system. The gain margins corresponding to $K_\alpha = 1$ and $K_\alpha = 1.5$ kg m^2 are, respectively, 1.318 and 0.858. Therefore, the former gain results in a stable coupled system, and the latter in an unstable one.

For the filter with cut-off frequency $\omega_{lo} = 10$ rad/s, the transition from a stable to an unstable coupled system occurs at $K_\alpha = 1.22$ kg m^2. Considering a typical inertia moment value $I_h = 3.38$ kg m^2 for the human leg (Appendix A), said value of K_α corresponds to a virtual inertia moment of 2.16 kg m^2 at low frequencies. Thus, for this particular filter, the maximum reduction in moment of inertia before instability occurs is about 36%.

3.4. Optimization to achieve a desired assistance

We present now a method for obtaining an optimal control for the exoskeleton. Given a range of motion frequencies $[0, \omega_f]$, our chosen objective is for the coupled human–exoskeleton system to exhibit a desired assistance ratio $\mathcal{A}(\omega_f) = \mathcal{A}_d$, along with zero resistance ratio. In other words, for any frequency $\omega \in [0, \omega_f]$, the integral admittance magnitude can only increase or stay the same. The optimal set of control parameters for the exoskeleton is obtained by solving the following constrained optimization:

$$\begin{aligned} \underset{\{K_\theta, K_\omega, K_\alpha, \omega_{lo}\}}{\text{minimize}} \quad & |\mathcal{A}(\omega_f) - \mathcal{A}_d|^2 + w\mathcal{R}(\omega_f) \\ \text{subject to} \quad & GM(L_{heu}(j\omega)) > 1, \\ & \angle X_{heu}(j\omega) \in [-180°, 0°] \quad \forall \omega, \\ & \frac{|\zeta_{heu} - \zeta_h|}{\zeta_h} < \epsilon. \end{aligned} \tag{28}$$

The optimization (28) finds the parameters of the exoskeleton control law (26), namely, gains on the exoskeleton angle (K_θ), angular velocity (K_ω) and filtered acceleration (K_α), as well as the cut-off frequency ω_{lo} of the low-pass Butterworth filter in (27). The objective is to minimize the weighted sum of assistance ratio squared error and resistance ratio. The optimization finds

Please cite this article in press as: U. Nagarajan, et al., Integral admittance shaping: A unified framework for active exoskeleton control, Robotics and Autonomous Systems (2015), http://dx.doi.org/10.1016/j.robot.2015.09.015

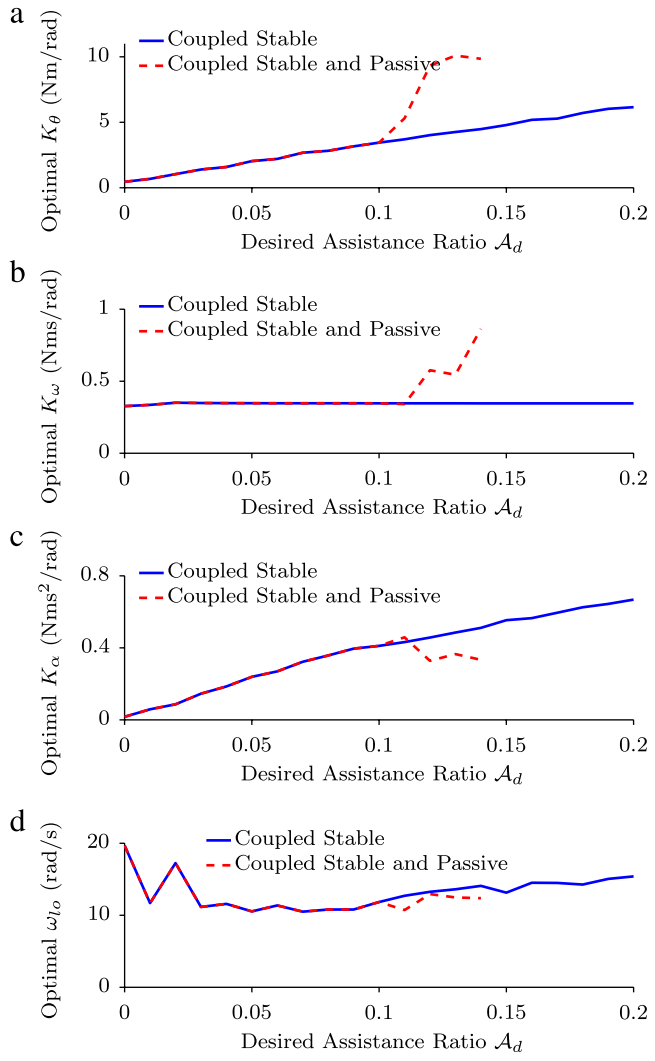

Fig. 6. Optimal control parameters needed to achieve $\mathcal{A}_d \in [0, 0.2]$ with and without passivity constraints: (a) K_θ, (b) K_ω, (c) K_α and (d) ω_{lo}. For desired assistance $\mathcal{A}_d > 0.1422$, the control parameters obtained without passivity constraints result in a closed-loop coupled human–exoskeleton system that is stable but not passive.

the solution while satisfying hard constraints for stability (16), passivity (17) and comfort (22).

We solve the constrained optimization by means of a Nelder–Mead simplex algorithm, which is a heuristic search method that uses only function evaluations. We chose this algorithm because of the difficulty of deriving analytical expressions for the assistance ratio $\mathcal{A}(\omega_f)$, resistance ratio $\mathcal{R}(\omega_f)$ and their gradients with respect to the control parameters. Given a current set of control parameters, the resulting assistance ratio $\mathcal{A}(\omega_f)$ can be calculated using (13), (18) and (19). With this, the cost functional in (28) can be evaluated. It should be noted that the "zero resistance ratio" condition is included as a soft constraint with a weighting term w. This avoids convergence problems that may result in the Nelder–Mead simplex from enforcing $\mathcal{R}(\omega_f) = 0$ as a hard constraint. For an n-dimensional optimization, the Nelder–Mead simplex starts with $n+1$ sets of initial parameters. These sets form the vertices of an $n+1$ polytope in the n-dimensional search space. Based on the cost function values at these vertices, the algorithm moves and shrinks these vertices towards the local optimum. More details can be found in [45].

Optimizations were performed in Matlab using the *fminsearch*() function, which employs the Nelder–Mead simplex. For all results in this paper, $\omega_f = 10$ rad/s was used. The human joint, exoskeleton and coupling parameters used to compute $X_h(j\omega)$ (7) and $X_{heu}(j\omega)$ (13) are given in Appendix A.

Fig. 6 shows the derived optimal control parameters for different desired assistance ratios $\mathcal{A}_d$ with and without the passivity constraint. In order to generate these results, the optimal control parameters for $\mathcal{A}_d = 0$ were obtained first. These were then employed as the initial parameter estimates for $\mathcal{A}_{d,1} = \mathcal{A}_d + 0.01$. From there we proceeded in a recursive manner, using the optimal parameters for $\mathcal{A}_{d,k}$ as the initial estimates for $\mathcal{A}_{d,k+1} = \mathcal{A}_{d,k} + 0.01$. (Functional tolerance was 10^{-5}.)

When passivity was not enforced, the optimization algorithm found control parameters that achieved desired assistance ratios in the range $\mathcal{A}_d \in [0, 1]$ while guaranteeing stability. By contrast, when passivity was enforced, valid solutions could only be found for assistance ratios up to $\mathcal{A}_d = 0.1422$. This value represents a theoretical limit to the level of assistance that the leg can handle; for any assistance ratio up to $\mathcal{A}_d = 0.1422$ it is guaranteed that the leg will not lose stability when in contact with an external (passive) environment, such as a compliant floor surface.

Fig. 7 shows the Nyquist plots of $L_{heu}(s)$ for several target values of $\mathcal{A}_d$ and their corresponding optimal control parameters. None of the Nyquist plots encircle -1, thereby emphasizing that the derived coupled human–exoskeleton systems are all stable irrespective of whether they are passive (Fig. 7(a)) or active (Fig. 7(b)).

Fig. 8(a) shows the integral admittance magnitude of the coupled human–exoskeleton system for different values of $\mathcal{A}_d$ in the passive range. The integral admittance magnitude $|X_h(j\omega)|$ of the unassisted leg is shown for comparison. As should be expected, $|X_h(j\omega)|$ is nearly identical to the integral admittance magnitude $|X_{heu}(j\omega)|$ of the coupled system when $\mathcal{A}_d = 0$. The corresponding assistance function profiles $\mathcal{AF}(\omega)$ are shown in Fig. 8(b). It can be seen that $\mathcal{AF}(\omega)$ starts close to zero at lower frequencies, peaks near the resonant frequency of $X_{heu}(j\omega)$, and then rolls off towards zero at higher frequencies. Thus it is likely that assistance as perceived by the user will be maximal when moving the leg at a frequency near resonance.

4. Robust stability, passivity and performance analysis

This section presents a detailed analysis of the robust stability, passivity and performance margins of the exoskeleton controllers derived using integral admittance shaping.

4.1. Robust stability and passivity

While exoskeleton parameters $\{I_e, b_e, k_e\}$ can be estimated quite accurately, the human parameters $\{I_h, b_h, k_h\}$ and the coupling parameters $\{b_c, k_c\}$ are subject to considerable variation. Although the passive stiffness of the hip joint can be estimated with reasonable accuracy under highly controlled conditions [46], in practice it is subject to reflexive components due to muscle activation [47]. Likewise, the coupling compliance parameters can vary during motion. These uncertainties demand the exoskeleton control to be highly robust to parameter variations.

The nominal parameter values are shown in Appendix A. We represent the human, exoskeleton and coupling parameter values normalized with respect to their nominal values as $\{\hat{I}_h, \hat{b}_h, \hat{k}_h, \hat{I}_e, \hat{b}_e, \hat{k}_e, \hat{b}_c, \hat{k}_c\}$. Fig. 9 presents the normalized parameters' lower bounds for simultaneous stability and passivity using the condition (17). In each case, only one parameter is varied and the remaining parameters are maintained at their nominal values.

By contrast, there are no upper bounds to the stability and passivity margin, i.e. the upper bounds are $+\infty$. In other words, as the human limb, exoskeleton and coupling increase in stiffness, damping or inertia, their impedance increases and as a result, and

Please cite this article in press as: U. Nagarajan, et al., Integral admittance shaping: A unified framework for active exoskeleton control, Robotics and Autonomous Systems (2015), http://dx.doi.org/10.1016/j.robot.2015.09.015

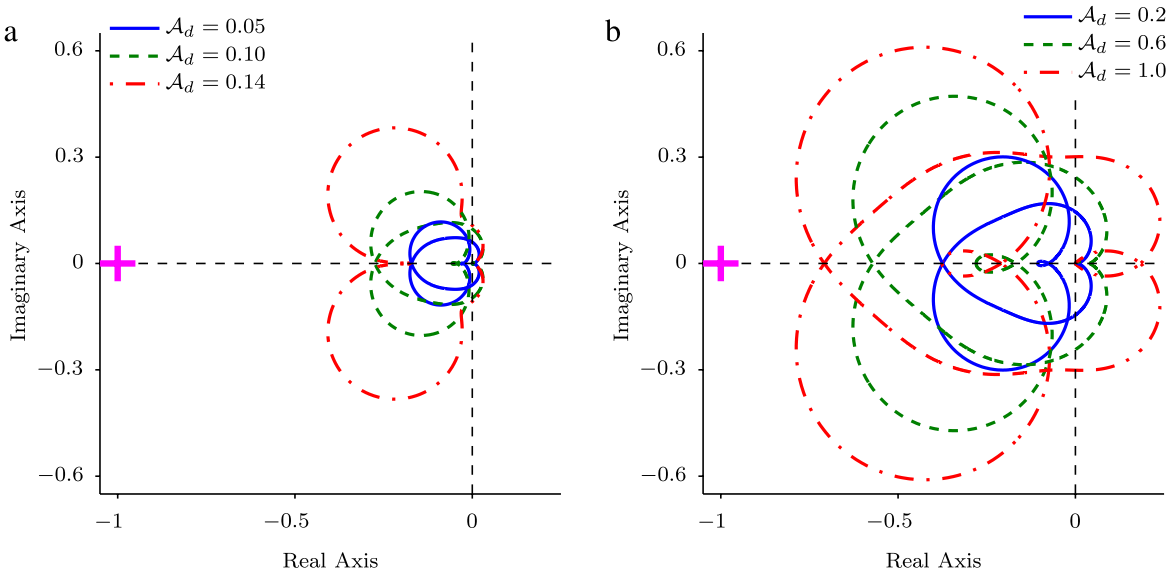

Fig. 7. Nyquist plots of $L_{heu}(s)$ for the optimal control parameters in Fig. 6 that achieve coupled stability (a) with the passivity constraint, and (b) without the passivity constraint. None of the Nyquist plots encircle −1 resulting in stable coupled human–exoskeleton systems.

the coupled human–exoskeleton system becomes more stable and passive. This indicates that it is generally better to underestimate the parameters than to overestimate them, as underestimating only allows for positive variations.

Fig. 9 provides a general view of the system's sensitivity to both parameter variations and the assistance ratio, $\mathcal{A}_d$. Overall, stability and passivity robustness tend to decrease as the assistance ratio increases. This is especially the case for variations in human damping b_h. When $\mathcal{A}_d \geq 0.1$, there is also a considerable reduction in robustness to variations in exoskeleton damping b_e and coupling stiffness k_c. By contrast, there is consistently large robustness to variations in moment of inertia (either I_h or I_e), human joint stiffness k_h and coupling damping b_c.

4.2. Robust performance

Although stability and passivity are guaranteed for a wide range of parameter variations, this does not necessarily guarantee that the desired assistance is achieved. Therefore it is necessary to consider performance robustness as well. In order to provide a performance criterion, we define the controller as having robust performance if, for a given parameter variation, the absolute variations in assistance ratio and resistance ratio are within 2%, i.e., $\Delta\mathcal{A} \leq 0.02$ and $\Delta\mathcal{R} \leq 0.02$.

Fig. 10 presents the lower and upper bounds of the normalized dynamics parameters $\{\hat{I}_h, \hat{b}_h, \hat{k}_h, \hat{I}_e, \hat{b}_e, \hat{k}_e, \hat{b}_c, \hat{k}_c\}$ for which robust performance is guaranteed when the optimal control parameters are used. Only parameter variations that guarantee stability and passivity (Fig. 9) are considered here. When one parameter is varied, the rest are maintained at unity.

Fig. 10(d), (f) and (g) show that the coupled system's performance is highly robust to variations in exoskeleton moment of inertia I_e, exoskeleton stiffness k_e and coupling damping b_c. The human joint stiffness k_h, exoskeleton damping b_e and coupling stiffness k_c only affect the performance significantly for desired assistance ratios $\mathcal{A}_d \geq 0.1$, as shown in Fig. 10(c), 10(e) and 10(h) respectively. The lowest performance robustness occurs for variations in human inertia I_h and human damping b_h (Fig. 10(a) and (b)).

5. Initial trials

Our assistive control method is unconventional in that it destabilizes the exoskeleton arm by design (on account of the positive feedback), but allows the coupled system formed by the leg and the exoskeleton to remain stable and passive on account of the legs own passive dynamics. We ran a few experimental trials to test the feasibility of walking stably in an exoskeleton using our proposed control. Full experimental validation of the kinematic and physiological effects of the exoskeleton control on human gait will be the object of a future study involving a larger number of participants walking with and without the exoskeleton under controlled conditions [48].

Two adult male subjects walked in an experimental powered exoskeleton that uses our proposed control. (Subject 1: height 165 cm, weight 65 kg; subject 2: height 181 cm, weight 76 kg.) For each experimental condition, the subjects walked at their normal paces in a straight line for about 14 m. The device, shown in Fig. 1, features two flat brushless motors concentric with the axis of the hip joints on the sagittal plane. The motors exert torque on the user's legs through a pair of rigid, lightweight arms coupled to the thighs. A back support was added to the original exoskeleton design to provide a more rigid attachment to the human torso. The system parameters of the exoskeleton are given in Appendix A. Each motor has a Hall-effect sensor that measures the exoskeleton joint angle θ_e; the motor's maximum torque output is 6 N m. In order to make adaptation to the exoskeleton easy, and given the limited torque capacity of the device, we limited the assistance ratio $\mathcal{A}_d$ to a maximum 0.05.

Fig. 11 shows the block diagram of the exoskeleton control. The control parameters $\{K_\alpha, K_\omega, K_\theta, \omega_{lo}\}$ are obtained from the optimization in Section 3.4. A model-free Kalman filter [49] is used to estimate the exoskeleton joint angle θ_e, angular velocity $\dot{\theta}_e$ and angular acceleration $\ddot{\theta}_e$ needed to implement the control law (26).

Subjects reported no difficulty walking with the exoskeleton control. Fig. 12 presents the hip joint phase plots ($\hat{\theta}_e$ vs. $\dot{\hat{\theta}}_e$) for four different conditions, namely, passive (unpowered) device, zero assistance while powered ($\mathcal{A}_d = 0$), and two non-zero desired assistance ratios ($\mathcal{A}_d = 0.02, 0.05$). Fig. 12 shows that, for both subjects, the phase plot corresponding to $\mathcal{A}_d = 0$ has larger amplitude than the one corresponding to the passive exoskeleton. This reflects the fact that the passive exoskeleton increases the impedance of the human leg, whereas with $\mathcal{A}_d = 0$, the active exoskeleton is able to recover the original human limb dynamics. It can also be seen that, for both subjects, the amplitude of the

Please cite this article in press as: U. Nagarajan, et al., Integral admittance shaping: A unified framework for active exoskeleton control, Robotics and Autonomous Systems (2015), http://dx.doi.org/10.1016/j.robot.2015.09.015

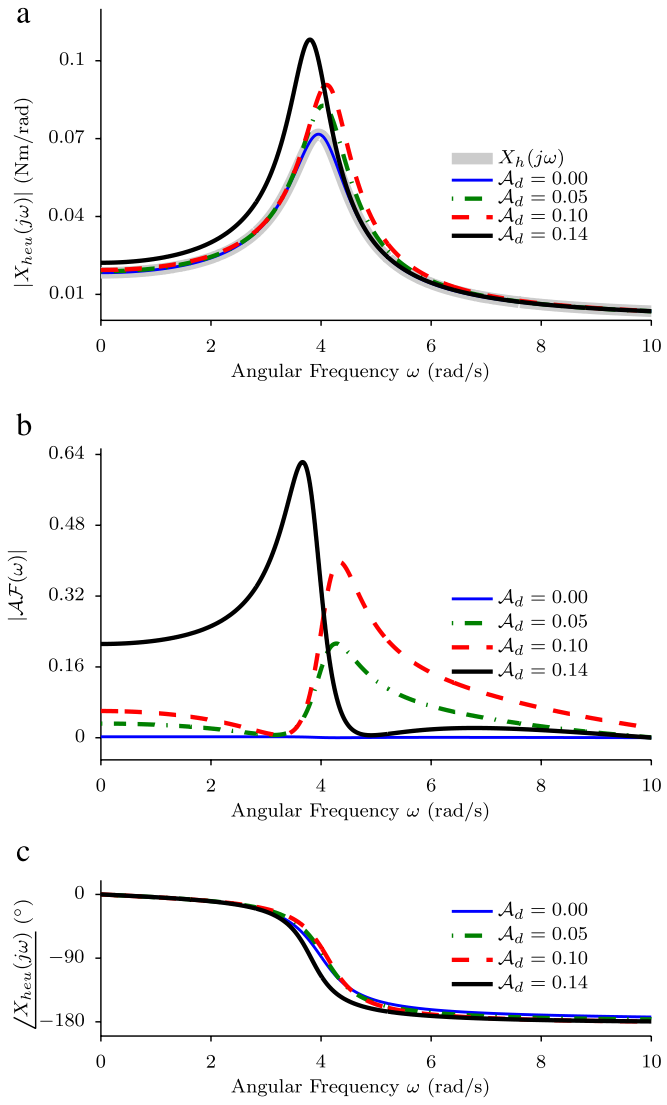

Fig. 8. Coupled human–exoskeleton system with control parameters optimized to achieve coupled stability and passivity. In this optimization example, the maximum motion frequency considered was $\omega_f = 10$ rad/s. (a) Integral admittance magnitude $|X_{heu}(j\omega)|$ of the coupled system, for different assistance ratios $\mathcal{A}_d$. (b) Assistance functions $\mathcal{AF}(\omega)$ (19) for the different values of $\mathcal{A}_d$. (The assistance ratio is equal to the area under $\mathcal{AF}(\omega)$ divided by ω_f.) (c) Integral admittance phase $\angle X_{heu}(j\omega)$ for the different values of $\mathcal{A}_d$. The phase values are strictly in the $[-180°, 0°]$, indicating that the coupled system is passive.

phase plot further increases as the assistance ratio $\mathcal{A}_d$ goes to 0.02 and then to 0.05. Thus it appears that, in the absence of external references for the subjects to follow, the subject's initial response to the exoskeleton control will be one of motion amplification (Section 3.1), i.e. increased amplitude of the hip joint's angular motion, with net muscle torque relatively unchanged.

The time trajectories of the exoskeleton torque τ_e acting on the left leg are shown in Fig. 13, along with the time trajectories of the angular velocity $\dot{\theta}_e$ and angular position θ_e. The torque trajectories corresponding to $\mathcal{A}_d = 0.05$ saturate at 6 N m. For this reason, controllers achieving larger assistance ratios ($\mathcal{A}_d > 0.05$) were not tested. Again, the main observable difference between conditions was an increase in motion amplitude, which translates into a larger stride length. It can also be noticed that the exoskeleton torque is nearly in phase with the angular velocity. This is consistent with the integral admittance profile shown in Fig. 8(a) for $\mathcal{A}_d = 0.05$; the main difference with respect to the unassisted case ($\mathcal{A}_d = 0$) is a decrease in the damping ratio of the leg. Thus the exoskeleton behaves mainly as a damping reduction device, i.e. a negative damper, which explains the observed phase synchronization between the torque and the angular velocity.

6. Discussion and conclusions

We have presented conceptual and quantitative definitions of assistance and resistance based on the frequency response of a linearized human limb model. An exoskeleton control is considered to be assistive if the admittance magnitude of the coupled human limb–exoskeleton system is larger than that of the unassisted limb over a certain frequency interval. We introduced *integral admittance shaping*, a control design framework based on shaping the frequency response magnitude profile of the system's integral admittance. The control ensures that the coupled system is stable and passive, thereby guaranteeing stable interaction with passive environments.

Integral admittance shaping was formulated as a constrained optimization problem that finds the optimal exoskeleton control parameters that achieve the desired assistance ratio and at the same time enforce stability, passivity and comfort constraints. We also presented a detailed robustness analysis of the exoskeleton control to parameter uncertainties, together with results from a first trial with Honda's Stride Management Assist device that demonstrated amplification of hip joint motion during walking.

Although our experimental data is quite limited in scope, the observed increase in hip angle amplitude is consistent with the theoretical profile of the integral admittance of the leg–exoskeleton system. In Fig. 8(a), the frequency response for $\mathcal{A}_d = 0.05$ can be seen mainly as a virtual decrease in the damping ratio of the leg. Assuming subjects prefer to walk at leg-swing frequencies near resonance, for a given muscle torque it can be expected to see a larger swing amplitude.

The larger hip excursions observed in the trials also seem consistent with data from experiments involving other forms of assistive control, such as the oscillator-driven control reported in [36]. At the same time, it needs to be determined if, with sufficient training, subjects can learn to reduce their muscle activation in response to the assistive torque from the exoskeleton, i.e. make the transition to a "torque reduction" condition. Achieving consistent reductions in muscle activation typically requires trial durations in the order of 30 min [17,19].

We now discuss two important facts, which are useful in designing exoskeleton controllers using the integral admittance shaping framework.

6.1. Same desired assistance ratio can be achieved by an infinite set of integral admittance shapes

The control parameters generated by the optimization (28) depend on the chosen initial parameter values as well as the constraints used. As a consequence, there are an infinite number of integral admittance profile shapes that can produce the same assistance ratio. Thus an open question is how to choose among these shapes.

For the results presented in Fig. 6, the optimal control parameters for $\mathcal{A}_d = 0$ were obtained first, and then used as initial parameter values for the case $\mathcal{A}_d$+0.01. Generation of optimal controllers then proceeded in a recursive manner. As a result, the optimization (28) produced integral admittance profiles that did not depart too radically from the profile corresponding to the unassisted leg (Fig. 8).

Therefore, for a given assistance ratio, the designer could use additional constraints to choose from the infinite set of solutions. For example, and similar to the constraint on damping ratio in (22), constraints on natural frequency and resonant peak magnitude could be added to (28) to restrict the set of acceptable solutions.

Please cite this article in press as: U. Nagarajan, et al., Integral admittance shaping: A unified framework for active exoskeleton control, Robotics and Autonomous Systems (2015), http://dx.doi.org/10.1016/j.robot.2015.09.015

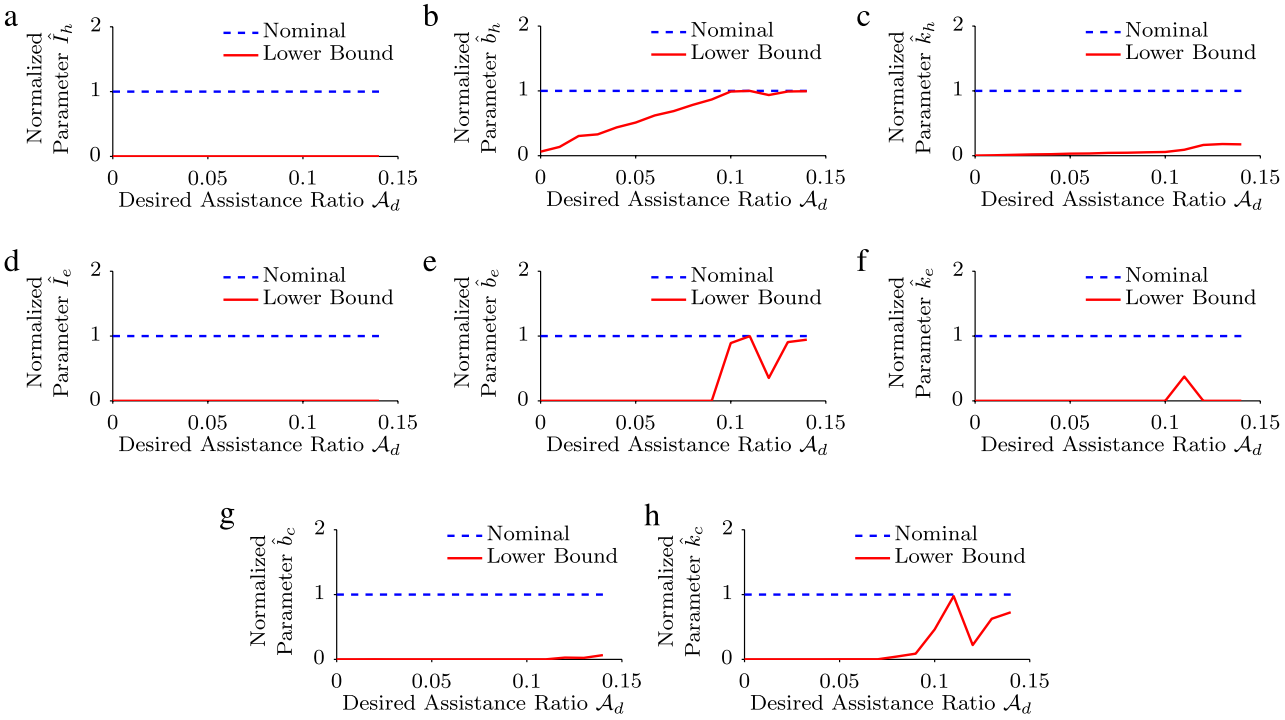

Fig. 9. Stability and passivity robustness. Graphs show the lower bounds for the variations of the normalized system parameters that the coupled human–exoskeleton system can handle while maintaining coupled stability and passivity. For each parameter variation, the other parameters are maintained at unity. There is no upper bound for the robust stability and passivity margin because as the human limb, exoskeleton and coupling become stiffer, more damped or more massive, their impedance increases and as a result, the coupled human–exoskeleton system becomes more passive and stable.

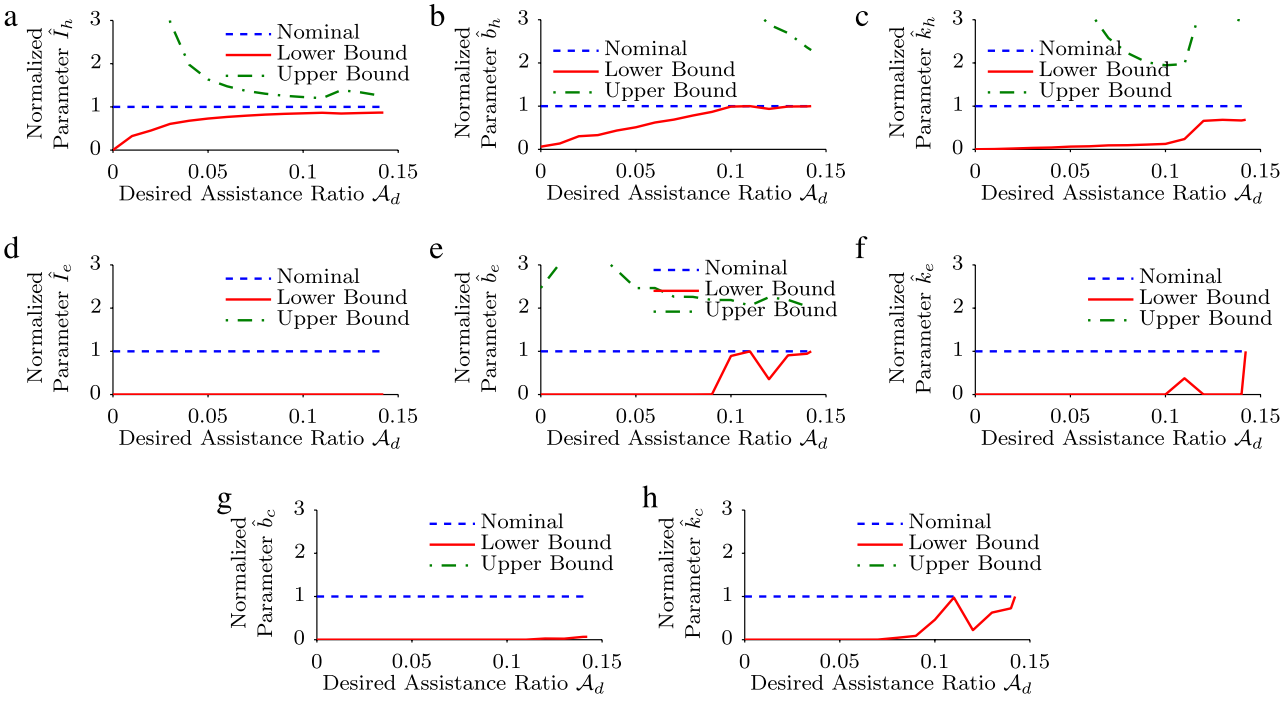

Fig. 10. Performance robustness. Graphs show the lower and upper bounds for variations of the normalized system parameters, which the coupled human–exoskeleton system can handle while achieving the desired assistance and resistance ratios within a tolerance of 2%, i.e., $\Delta\mathcal{A} \leq 0.02$ and $\Delta\mathcal{R} \leq 0.02$. For each parameter variation, the other parameters are maintained at unity, and only those parameter values that guarantee coupled stability and passivity are considered here. Only upper bounds $\leq$3 ($\leq$300%) are shown in the plots.

6.2. Desired integral admittance shapes can be directly chosen

The integral admittance shaping framework is not limited to the definitions of assistance and resistance presented in this paper. For certain applications, a desired integral admittance profile can be directly provided by the control designer. For example, the desired profile might correspond to an increase in natural frequency while maintaining the same damping ratio and resonant peak magnitude

Please cite this article in press as: U. Nagarajan, et al., Integral admittance shaping: A unified framework for active exoskeleton control, Robotics and Autonomous Systems (2015), http://dx.doi.org/10.1016/j.robot.2015.09.015

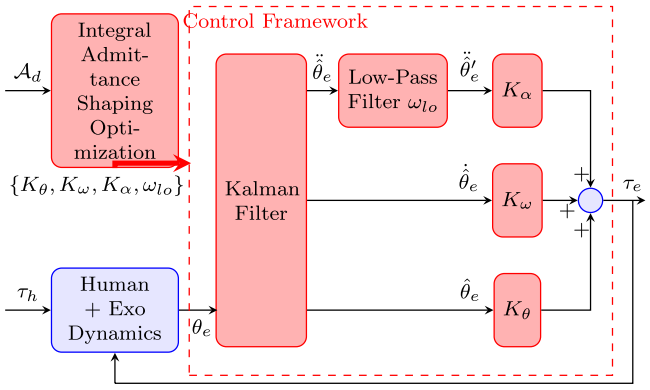

Fig. 11. Block diagram of the integral admittance shaping control.

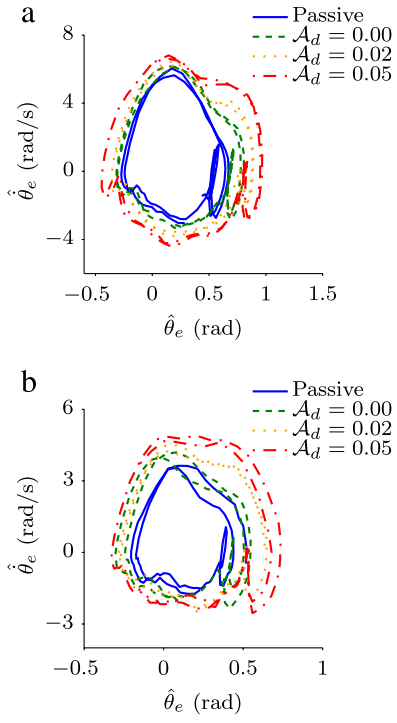

Fig. 12. Experimental results: Hip joint phase plots for different desired assistance ratios for two human subjects with (a) height = 165 cm, weight = 65 kg and (b) height = 181 cm, weight = 76 kg.

of the unassisted limb. In this case, the resistance ratio will be non-zero ($\mathcal{R}(\omega_f) \neq 0$), and the soft constraint on the resistance ratio (28) has to be removed.

Moreover, the integral admittance shaping framework can also be used to design resistive exoskeleton controllers. The desired exoskeleton behavior could be defined to have positive resistance ratio ($\mathcal{R}(\omega_f) > 0$) and zero assistance ratio ($\mathcal{A}(\omega_f) = 0$), and the optimization in (28) can be modified accordingly.

6.3. Future work

Future work will extend our formulation of assistance and resistance to multiple degrees of freedom. By virtue of the coupled joint dynamics, the exoskeleton can affect the movement of a given human joint even when there is no corresponding actuated exoskeleton joint. For example, the exoskeleton torque acting on the hip joint during the swing phase contributes to knee extension as well. Therefore we plan to develop a general formulation of integral admittance shaping for multiple-input multiple-output (MIMO) systems.

Moreover, the definitions and approach presented in this paper can also be extended to include task-level assistance rather than joint-level assistance. For such a case, a task-level output such as the Cartesian position of the foot can be chosen.

For the purposes of stability and performance robustness, a more realistic model of the human joints' reflexive impedance will be used in the human limb model. We also plan to study the physiological effects of the integral admittance shaping control on the human user, specifically on muscle activation (EMG) and metabolic cost of walking.

Acknowledgment

The facilities and experimental equipment for this project were provided by the Honda Research Institute, USA.

Appendix A. System parameters

The following human limb and exoskeleton parameters were used in the analysis and tests presented in this paper:

- Human Leg Mass: $m_h = 10.47$ kg.
- Human Leg Length: $l_h = 0.875$ m.
- Human Leg Moment of Inertia: $I_h = 3.38$ kg m^2
- Hip Joint Damping Coefficient: $b_h = 3.5$ N m s/rad.
- Hip Joint Stiffness Coefficient: $k_h = 54.7$ N m/rad.
- Human Leg Natural Frequency: $\omega_{nh} = 4.02$ rad/s.
- Exoskeleton Arm Moment of Inertia: $I_e = 0.01178$ kg m^2.
- Exoskeleton Shaft Damping Coefficient: $b_e = 0.345$ N m s/rad.
- Exoskeleton Shaft Stiffness Coefficient: $k_e = 0.339$ N m/rad.
- Coupling Damping Coefficient: $b_c = 9.47$ N m s/rad.
- Coupling Stiffness Coefficient: $k_c = 1905$ N m/rad.

The human limb data are average values for a human male with a weight of 65 kg and a height of 165 cm. Here, the knee joint is assumed to fully extended and all parameters are computed for the hip joint. The moment of inertia I_h is obtained from cadaver data in [50], and is scaled to the human weight and height. The joint damping coefficient is taken from [51], and the joint stiffness coefficient is obtained using $k_h = I_h\omega_{nh}^2$ where the natural frequency ω_{nh} is obtained from [52].

The exoskeleton parameters listed were obtained from system identification experiments performed on the experimental device (Fig. 1). The coupling parameters were obtained assuming second-order dynamics with a damping ratio $\zeta_c = 1$ and natural frequency $\omega_{nc} = 100\,\omega_{nh}$.

Appendix B. Inertia reduction cannot be achieved using only positive acceleration feedback

The moment of inertia of the coupled system could in theory be made less than that of the unassisted human limb by using positive feedback of the exoskeleton's angular acceleration $\ddot{\theta}_e$. However, the requirement for coupled stability requirement limits the amount of inertia that can be compensated by the exoskeleton controller. This section finds the stability limit for the case when pure positive acceleration feedback is used.

In (24), with no loss of generality, let us assume $b_e^d = b_e$, $k_e^d = k_e$. In order to emulate a negative inertia ($I_e^d < 0$), the exoskeleton control (23) reduces to

$$U_e(s) = K_\alpha s \tag{B.1}$$

where K_α is a positive acceleration feedback gain given by

$$K_\alpha = I_e - I_e^d. \tag{B.2}$$

In order to evaluate the system's stability when using the control (B.1), the system block diagram in Fig. 3(a) is converted to

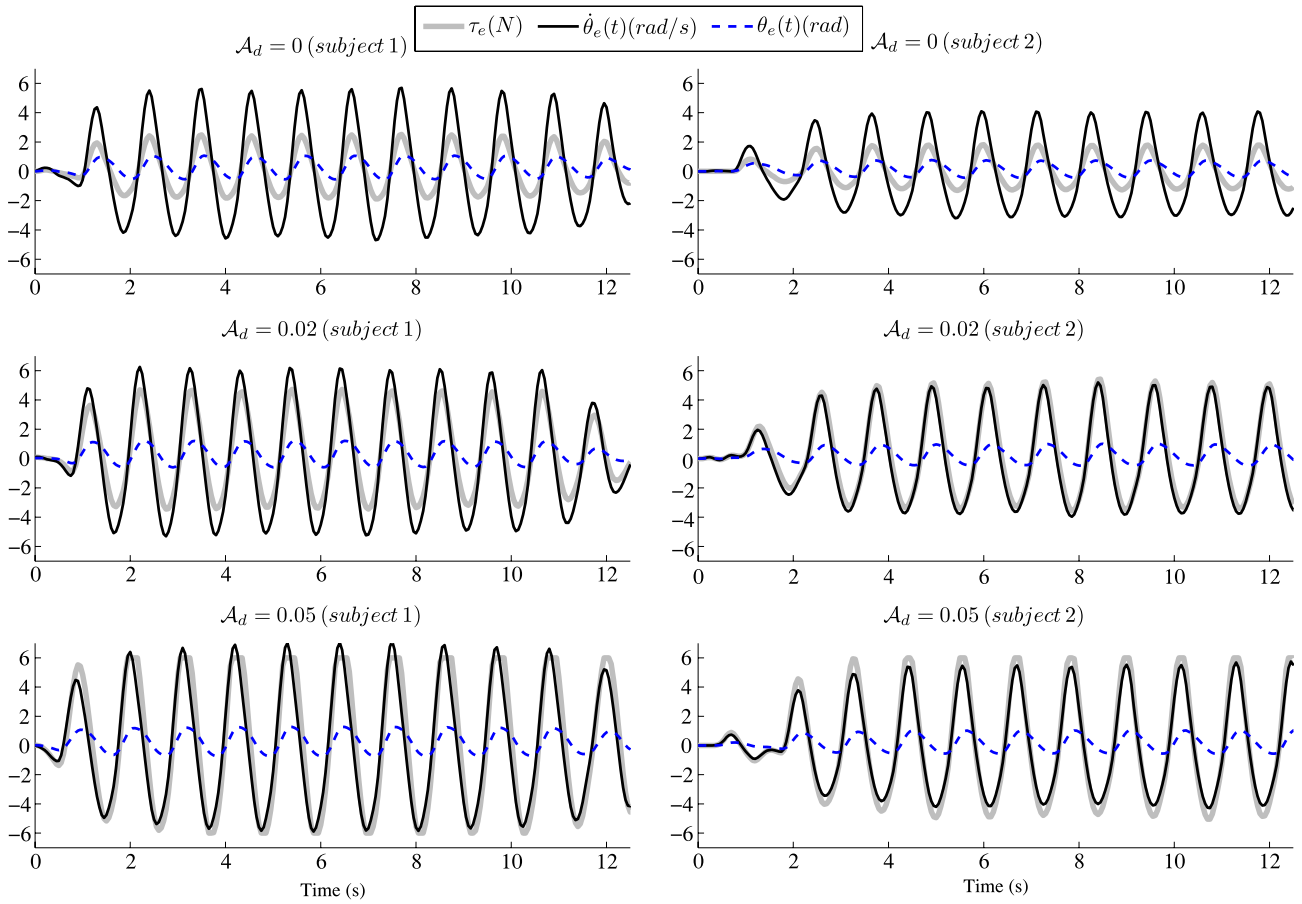

Fig. 13. Experimental trial with the powered exoskeleton: time trajectories for exoskeleton torque τ_e, angular velocity $\dot{\theta}_e$ and angular position θ_e under three assistance levels, $\mathcal{A}_d = 0$, 0.02 and 0.05.

the one in Fig. B.14, which features a single positive feedback loop and contains the following transfer functions:

$$S_{hc}(s) = \frac{Y_h(s)Z_c(s)}{1 + Y_h(s)Z_c(s)}, \tag{B.3}$$

$$Y_{he}(s) = \frac{Y_e(s)}{1 + Y_e(s)Z_{hc}(s)}. \tag{B.4}$$

Since $S_{hc}(s)$ in (B.3) is composed of two passive systems, the human and the coupling, it is always stable. Therefore, the stability of the system depends only on the stability of the feedback loop in Fig. B.14. The transfer function of the loop gain $L_{he}(s)$ used for the stability analysis of this feedback loop is given by

$$L_{he}(s) = s\, Y_{he}(s). \tag{B.5}$$

Because *positive* feedback is used (Fig. B.14), one needs to compute the gain margin of $-L_{he}(s)$ in order to evaluate the stability of the closed-loop system:

$$GM(L_{he}) = \frac{1}{\left|L_{he}(j\omega_c)\right|}, \tag{B.6}$$

where ω_c is the phase-crossover frequency i.e. the one satisfying $\angle{-L_{he}(j\omega_c)} = 180°$. The gain margin $GM(-L_{he})$ is equal to the maximum positive gain K_α (B.2), exceeding which the closed-loop system becomes unstable.

The phase-crossover frequency is computed from

$$\begin{aligned}\angle{-L_{he}(j\omega)} &= \angle{-Y_{he}(j\omega)} + \angle{j\omega} \\ &= \angle{-Y_{he}(j\omega)} + 90°.\end{aligned} \tag{B.7}$$

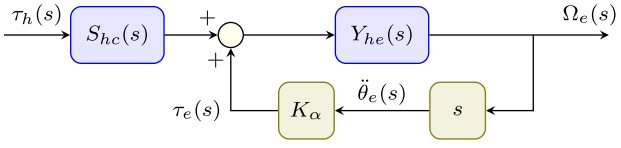

Fig. B.14. Block diagram of the coupled human–exoskeleton system with pure acceleration feedback.

Since $Y_{he}(s)$ constitutes a passive admittance, we have $\angle{-Y_{he}(j\omega)} \in [-90°, 90°]$, and hence

$$\angle{-L_{he}(j\omega)} \in [0°, 180°], \quad \forall\omega \geq 0. \tag{B.8}$$

Therefore, the phase-crossover frequency ω_c of $-L_{he}(s)$ is

$$\omega_c\left(-L_{he}\right) = \infty. \tag{B.9}$$

Substituting terms in (B.5), it can be shown that $L_{he}(s)$ has the following equivalent form:

$$L_{he}(s) = \frac{I_h + \frac{a_1}{s} + \frac{a_0}{s^2}}{I_h I_e + \frac{b_3}{s} + \frac{b_2}{s^2} + \frac{b_1}{s^3} + \frac{b_0}{s^4}}. \tag{B.10}$$

Thus, for $s = j\omega_c = j\infty$, (B.10) reduces to

$$L_{he}(j\infty) = \frac{1}{I_e} \tag{B.11}$$

and, from (B.11), the gain margin of $-L_{he}(s)$ reduces to

$$GM(L_{he}) = I_e. \tag{B.12}$$

Thus the maximum allowable feedback gain K_α is equal to the exoskeleton's moment of inertia I_e, and is invariant with the parameters of the human joint and the coupling element. Therefore, for $K_\alpha > I_e$, the coupled human–exoskeleton system

Please cite this article in press as: U. Nagarajan, et al., Integral admittance shaping: A unified framework for active exoskeleton control, Robotics and Autonomous Systems (2015), http://dx.doi.org/10.1016/j.robot.2015.09.015

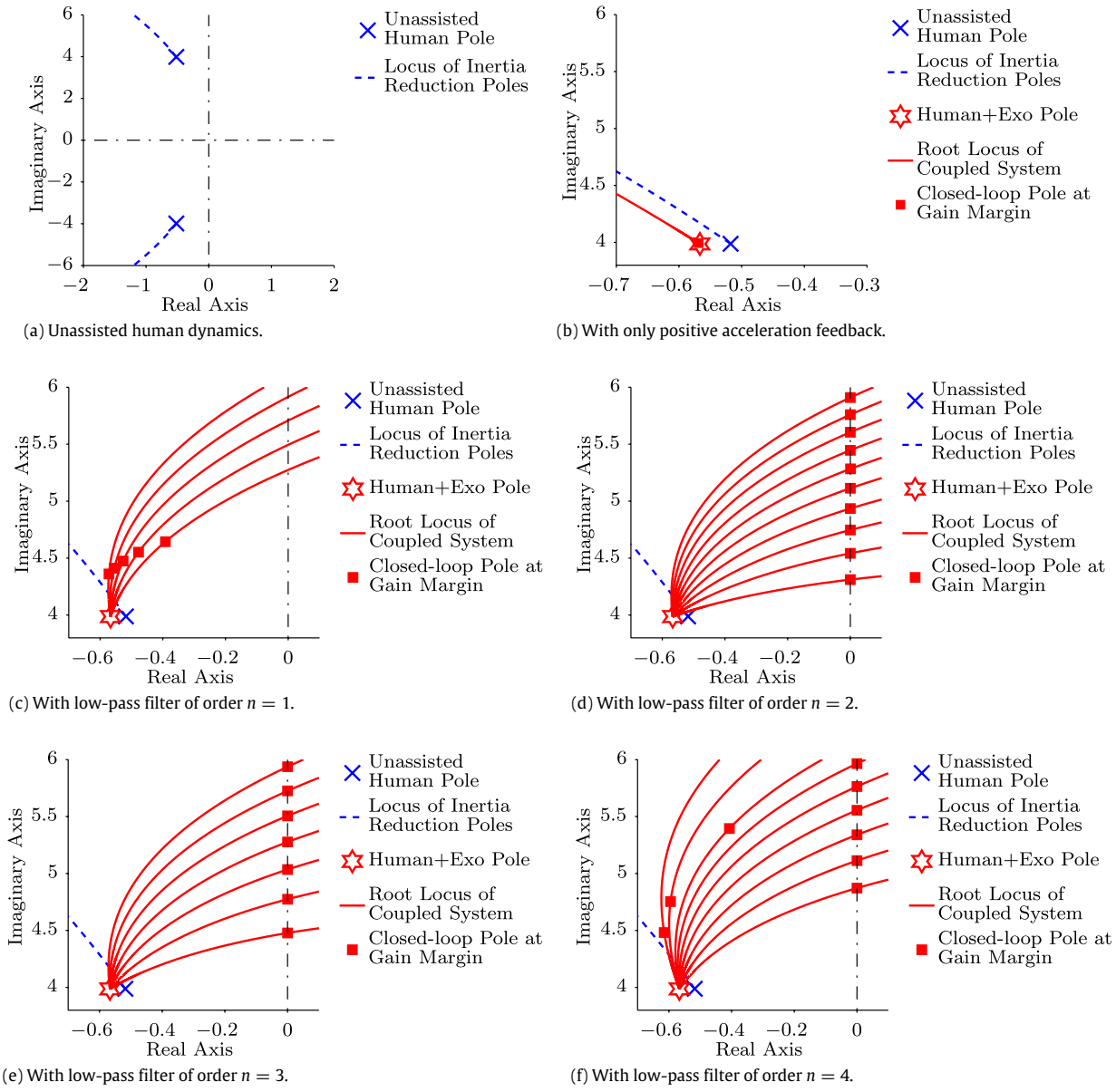

(a) Unassisted human dynamics.

(b) With only positive acceleration feedback.

(c) With low-pass filter of order $n = 1$.

(d) With low-pass filter of order $n = 2$.

(e) With low-pass filter of order $n = 3$.

(f) With low-pass filter of order $n = 4$.

Fig. C.15. Root locus plots of $-L_{he}(s)$ used to study the effect of adding low-pass Butterworth filters of different orders to the exoskeleton controller. Inertia reduction cannot be achieved using only positive acceleration feedback since the coupled system becomes unstable without any significant migration of the dominant closed-loop poles as shown in (b). Moreover, its root locus does not intersect the locus of inertia reduction poles. However, using low-pass filters, there are multiple root loci corresponding to different cut-off frequencies that intersect the locus of inertia reduction poles while guaranteeing coupled stability as shown in (c)–(f). The closed-loop poles corresponding to the gain margin of $-L_{he}(s)$ appear at gains larger than those required to achieve inertia reduction demonstrating that the coupled stability is guaranteed while achieving inertia reduction.

will be unstable regardless of how stiff or damped the coupling is. In consequence, with only positive acceleration feedback, the desired emulated moment of inertia I_e^d of the exoskeleton obtained from (B.2) cannot be negative as desired, and the moment of inertia of the coupled system cannot be reduced below that of the unassisted human.

Appendix C. Inertia reduction using low-pass filters

We explain now how a reduction in the moment of inertia of the human limb can be emulated by adding extra poles to the closed-loop transfer function.

Although the coupled human–exoskeleton system in (1)–(3) is fourth-order, its response is dominated by a pair of conjugate poles located near the poles of the unassisted human joint dynamics (6). Fig. C.15(a) shows the two poles corresponding to the unassisted human joint dynamics in the complex plane. It also shows the locus of these two poles as a hypothetical inertia reduction takes place, i.e., as I_h becomes progressively smaller.

In order to emulate inertia reduction, we need to shape the root locus of the coupled human–exoskeleton system in such a way that it intersects the locus of "inertia reduction" poles. At the same time, the stability of the coupled system must be guaranteed. This requires that the other parts of the coupled system's root locus do not enter the right-hand half of the complex plane.

We can modify the shape of the coupled system's root locus by adding poles to the loop transfer function. The simplest way to do so is by means of a low-pass filter. We examine now the effect of adding a low-pass Butterworth filter, the transfer function of which is given by

$$H_{lo}(s) = \frac{\omega_{lo}^n}{\prod_{k=1}^{n}(s - s_k)}, \tag{C.1}$$

Please cite this article in press as: U. Nagarajan, et al., Integral admittance shaping: A unified framework for active exoskeleton control, Robotics and Autonomous Systems (2015), http://dx.doi.org/10.1016/j.robot.2015.09.015

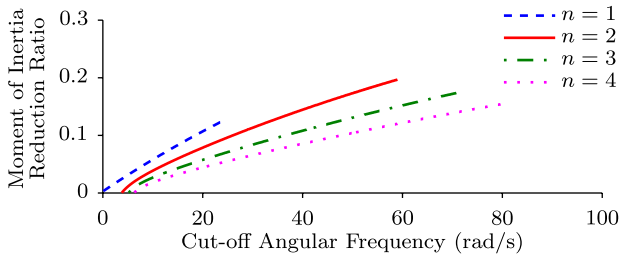

Fig. C.16. Achievable inertia reduction using low-pass Butterworth filters of different orders ($n = 1$ to $n = 4$) with increasing cut-off frequency. The limiting factor for inertia reduction is the stability of the coupled human–exoskeleton system.

where n is the order of the filter, ω_{lo} is the cut-off angular frequency and

$$s_k = \omega_{lo} e^{j\frac{(2k+n-1)\pi}{2n}}. \tag{C.2}$$

The number of poles added is equal to the order of the filter. Irrespective of the order, the Butterworth filter has only one tunable parameter, ω_{lo}.

Fig. C.15(c)–(f) shows root loci for the closed loop system with Butterworth filters added. Each graph corresponds to a Butterworth filter of different order ($n = 1$ through $n = 4$). Each graph includes root loci for different cut-off frequencies ω_{lo}. It can be seen that, in all cases, the root loci intersect the locus of the "inertia reduction" poles. This indicates that, with any Butterworth filter, it is possible to generate a pair of dominant closed-loop poles that match a pair of "inertia reduction" poles. By contrast, for pure acceleration feedback (Fig. C.15(b)) no such intersection occurs.

Critically, the above graphs also provide information about closed-loop stability. Fig. C.15(c)–(f) shows the closed-loop poles for a loop gain equal to the gain margin. It can be seen that, in all cases, the gain required to achieve inertia reduction is smaller than the gain margin. Therefore, by using low-pass filtered acceleration feedback, the exoskeleton controller can emulate inertia reduction while guaranteeing coupled stability.

Fig. C.16 shows plots of achievable inertia reduction (i.e., without loss of stability) for low-pass Butterworth filters of different orders and with different cut-off frequencies. There exists, for all filters, a range of cut-off frequencies for which non-zero inertia reduction can be achieved. It can also be seen that the achievable inertia reduction increases with cut-off frequency until it reaches a maximum.

We note in Fig. C.16 that the second-order low-pass filter is the one that achieves the maximum possible inertia reduction. Therefore we choose the second-order filter for the exoskeleton control law (26).

References

[1] D. Aoyagi, W. Ichinose, S. Harkema, D. Reinkensmeyer, J. Bobrow, A robot and control algorithm that can synchronously assist in naturalistic motion during body-weight-supported gait training following neurologic injury, IEEE Trans. Neural Syst. Rehabil. Eng. 15 (3) (2007) 387–400.
[2] J. Veneman, R. Kruidhof, E. Hekman, R. Ekkelenkamp, E. Van Asseldonk, H. van der Kooij, Design and evaluation of the LOPES exoskeleton robot for interactive gait rehabilitation, IEEE Trans. Neural Syst. Rehabil. Eng. 15 (3) (2007) 379–386.
[3] H. Kazerooni, R. Steger, Berkeley lower extremity exoskeleton, ASME J. Dyn. Syst. Meas. Control 128 (2006) 14–25.
[4] C.J. Walsh, K. Endo, H. Herr, A quasi-passive leg exoskeleton for load-carrying augmentation, Int. J. Humanoid Rob. 4 (3) (2007) 487–506.
[5] H. Kawamoto, Y. Sankai, Power assist system hal-3 for gait disorder person, in: Proc. Int. Conf. Comput. Helping People Special Needs, ICCHP, 2002, pp. 196–203.
[6] J.E. Pratt, B.T. Krupp, C.J. Morse, S.H. Collins, The RoboKnee: An exoskeleton for enhancing strength and endurance during walking, in: Proc. IEEE Int. Conf. Robotics and Automation, ICRA, 2004, pp. 2430–2435.
[7] K. Kiguchi, K. Iwami, M. Yasuda, K. Watanabe, T. Fukuda, An exoskeletal robot for human shoulder joint motion assist, IEEE/ASME Trans. Mechatronics 8 (1) (2003) 125–135.
[8] J.C. Perry, J. Rosen, S. Burns, Upper-limb powered exoskeleton design, IEEE/ASME Trans. Mechatronics 12 (4) (2007) 408–417.
[9] R.A.R.C. Gopura, K. Kiguchi, SUEFUL-7: A 7-dof upper limb exoskeleton robot with muscle-model-oriented emg-based control, in: Proc. IEEE/RSJ Int. Conf. Intelligent Robots and Systems, IROS, 2009, pp. 1126–1131.
[10] A.U. Pehlivan, O. Celik, M.K. O'Malley, Mechanical design of a distal arm exoskeleton for stroke and spinal cord injury rehabilitation, in: Proc. IEEE Int'l. Conf. Rehabil. Robot., ICORR, 2011.
[11] H.A. Quintero, R.J. Farris, M. Goldfarb, Control and implementation of a powered lower limb orthosis to aid walking in paraplegic individuals, in: Proc. IEEE Int. Conf. Rehabilitation Robotics, ICORR, 2011.
[12] T. Koyama, I. Yamano, K. Takemura, T. Maeno, Multi-fingered exoskeleton haptic device using passive force feedback for dextrous teleoperation, in: Proc. IEEE/RSJ Int. Conf. Intelligent Robots and Systems, IROS, 2002, pp. 2905–2910.
[13] A. Frisoli, F. Rocchi, S. Marcheschi, A. Dettori, F. Salsedo, M. Bergamasco, A new force-feedback arm exoskeleton for haptic interaction in virtual environments, in: Proc. First Joint Eurohaptics Conf. and World Haptics Conf., 2005, pp. 195–201.
[14] S. Marcheschi, F. Salsedo, M. Bergamasco, Body extender: Whole body exoskeleton for human power augmentation, in: Proc. IEEE Int. Conf. Robotics and Automation, ICRA, 2011, pp. 611–616.
[15] H. Kawamoto, S. Lee, S. Kanbe, Y. Sankai, Power assist method for hal-3 using emg-based feedback controller, in: Proc. IEEE Int. Conf. Syst., Man, Cybern., 2003, pp. 1648–1653.
[16] K.E. Gordon, C.R. Kinnaird, D.P. Ferris, Locomotor adaptation to a soleus emg-controlled antagonistic exoskeleton, J. Neurophysiol. 109 (7) (2013) 1804–1814.
[17] T. Lenzi, M. Carrozza, S. Agrawal, Powered hip exoskeletons can reduce the user's hip and ankle muscle activations during walking, IEEE Trans. Neural Syst. Rehabil. Eng. 21 (6) (2013) 938–948.
[18] D.P. Ferris, J.M. Czerniecki, B. Hannaford, An ankle-foot orthosis powered by artificial pneumatic muscles, J. Appl. Biomech. 21 (2) (2005) 189–197.
[19] G.S. Sawicki, D.P. Ferris, Mechanics and energetics of level walking with powered ankle exoskeletons, J. Exp. Biol. 211 (Pt. 9) (2008) 1402–1413.
[20] P. Malcolm, W. Derave, S. Galle, D. De Clercq, A simple exoskeleton that assists plantarflexion can reduce the metabolic cost of human walking, PLoS One 8 (2) (2013) e56137. http://dx.doi.org/10.1371/journal.pone.0056137.
[21] L.M. Mooney, E.J. Rouse, H.M. Herr, Autonomous exoskeleton reduces metabolic cost of human walking during load carriage, J. Neuroeng. Rehabil. 11 (80) (2014).
[22] A.M. Grabowski, H.M. Herr, Leg exoskeleton reduces the metabolic cost of human hopping, J. Appl. Physiol. 107 (3) (2009) 670–678.
[23] D.J. Ferris, G.S. Sawicki, Linking the mechanics and energetics of hopping with elastic ankle exoskeletons, J. Appl. Physiol. 113 (12) (2012) 1862–1872.
[24] A. Gams, T. Petric, T. Debevec, J. Babic, Effects of robotic knee exoskeleton on human energy expenditure, IEEE Trans. Biomed. Eng. 60 (6) (2013) 1636–1644.
[25] J.A. Norris, K.P. Granata, M.R. Mitros, E.M. Byrne, A.P. Marsh, Effect of augmented plantarflexion power on preferred walking speed and economy in young and older adults, Gait Posture 25 (4) (2007) 620–627.
[26] G.S. Sawicki, D.P. Ferris, Powered ankle exoskeletons reveal the metabolic cost of plantar flexor mechanical work during walking with longer steps at constant step frequency, J. Exp. Biol. 212 (1) (2009) 21–31.
[27] S. Lee, Y. Sankai, The natural frequency-based power assist control for lower body with hal-3, in: Proc. IEEE Int. Conf. Sys. Man Cyber., ICSMC, 2003, pp. 1642–1647.
[28] G. Aguirre-Ollinger, J.E. Colgate, M.A. Peshkin, A. Goswami, Design of an active one-degree-of-freedom lower-limb exoskeleton with inertia compensation, Int. J. Robot. Res. 30 (4) (2011) 486–499.
[29] C. Fleischer, C. Reinicke, G. Hommel, Predicting the intended motion with EMG signals for an exoskeleton orthosis controller, in: IEEE/RSJ International Conference on Intelligent Robots and Systems, 2005, pp. 2029–2034.
[30] H. Kawamoto, Y. Sankai, Power assist method based on phase sequence and muscle force condition for HAL, Adv. Robot. 19 (7) (2005) 717–734.
[31] C. Lewis, D. Ferris, Invariant hip moment pattern while walking with a robotic hip exoskeleton, J. Biomech. 44 (5) (2011) 789–793.
[32] S. Banala, S. Kim, S. Agrawal, J. Scholz, Robot assisted gait training with active leg exoskeleton (ALEX), IEEE Trans. Neural Syst. Rehabil. Eng. 17 (1) (2009) 2–8.
[33] G. Aguirre-Ollinger, J. Colgate, M. Peshkin, A. Goswami, Design of an active one-degree-of-freedom lower-limb exoskeleton with inertia compensation, Int. J. Robot. Res. 30 (4) (2011) 486–499.
[34] H. Vallery, A. Duschau-Wicke, R. Riener, Generalized elasticities improve patient-cooperative control of rehabilitation robots, in: IEEE International Conference on Rehabilitation Robotics ICORR 2009, June 23–26, Kyoto, Japan, 2009, pp. 535–541.
[35] T. Sugar, A. Bates, M. Holgate, J. Kerestes, M. Mignolet, P. New, R. Ramachandran, S. Redkar, C. Wheeler, Limit cycles to enhance human performance based on phase oscillators, J. Mech. Robot. 7 (1) (2015) 8. http://dx.doi.org/10.1115/1.4029336.
[36] R. Ronsse, T. Lenzi, N. Vitiello, B. Koopman, E. van Asseldonk, S.M. De Rossi, J. van den Kieboom, H. van der Kooij, M. Carrozza, A. Ijspeert, Oscillator-based assistance of cyclical movements: model-based and model-free approaches, Med. Biol. Eng. Comput. 49 (10) (2011) 1173–1185.
[37] G. Aguirre-Ollinger, Exoskeleton control for lower-extremity assistance based on adaptive frequency oscillators: Adaptation of muscle activation and movement frequency, Proc. Inst. Mech. Eng. H 229 (1) (2015) 52–68. http://dx.doi.org/10.1177/0954411914567213.
[38] Honda, Honda's stride management assist device. http://corporate.honda.com/innovation/walk-assist/.

Please cite this article in press as: U. Nagarajan, et al., Integral admittance shaping: A unified framework for active exoskeleton control, Robotics and Autonomous Systems (2015), http://dx.doi.org/10.1016/j.robot.2015.09.015

[39] Yaskawa, Yaskawa's ankle-assist walking device. http://www.yaskawa.co.jp/en/newsrelease/technology/6634.
[40] J.E. Colgate, N. Hogan, An analysis of contact instability in terms of passive physical equivalents, in: Proc. IEEE Int. Conf. Robotics and Automation, ICRA, 1989, pp. 404–409.
[41] J.E. Colgate, The control of dynamically interacting systems (Ph.D. thesis), Massachusetts Institute of Technology, Cambridge, MA, 1988.
[42] U. Nagarajan, G.A. Ollinger, A. Goswami, Integral admittance shaping for exoskeleton control, in: IEEE Int. Conf. Robotics and Automation, ICRA, 2015.
[43] G. Aguirre-Ollinger, Active impedance control of a lower-limb assistive exoskeleton (Ph.D. thesis), Northwestern University, Evanston, IL, 2007.
[44] G. Aguirre-Ollinger, J.E. Colgate, M.A. Peshkin, A. Goswami, A 1-DOF assistive exoskeleton with virtual negative damping: Effects on the kinematic response of the lower limbs, in: Proc. IEEE Int. Conf. Intelligent Robots and Systems, IROS, 2007, pp. 1938–1944.
[45] J. Nelder, R. Mead, A simplex method for function minimization, Comput. J. 7 (1964) 308–313.
[46] J. Fee, F. Miller, The leg drop pendulum test performed under general anesthesia in spastic cerebral palsy, Dev. Med. Child. Neurol. 46 (2004) 273–281.
[47] A. Schouten, E. Vlugt, F. Van der Helm, Design of perturbation signals for the estimation of proprioceptive reflexes, IEEE Trans. Biomed. Eng. 55 (5) (2008) 1612–1619.
[48] D. Ferris, G. Sawicki, M. Daley, A physiologist's perspective on robotic exoskeletons for human locomotion, Int. J. Humanoid Rob. 4 (2007) 507–528.
[49] P. Belanger, P. Dobrovolny, A. Helmy, X. Zhang, Estimation of angular velocity and acceleration from shaft-encoder measurements, Int. J. Robot. Res. 17 (11) (1998) 1225–1233.
[50] D.A. Winter, Biomechanics and Motor Control of Human Movement, fourth ed., Wiley, 2009, p. 86.
[51] K.C. Hayes, H. Hatze, Passive visco-elastic properties of the structures spanning the human elbow joint, Eur. J. Appl. Physiol. 37 (1977) 265–274.
[52] J. Doke, J.M. Donelan, A.D. Kuo, Mechanics and energetics of swinging the human leg, J. Exp. Biol. 208 (2005) 439–445.

Umashankar Nagarajan is a Roboticist at Google Inc., USA. Before joining Google, he worked as a Researcher at Honda Research Institute USA Inc. and as a Postdoctoral Associate at Disney Research, Pittsburgh, USA. He received his Ph.D. in robotics from The Robotics Institute of Carnegie Mellon University, Pittsburgh, USA. His research interests include exoskeletons, wheeled and legged balancing robots, underactuated systems, human–robot physical interaction and integrated planning and control.

Gabriel Aguirre-Ollinger is a Lecturer at the School of Electrical, Mechanical and Mechatronic Systems of the University of Technology, Sydney (UTS), Australia, and a core member of the UTS Centre for Autonomous Systems. He received a Master's degree from Carnegie Mellon University in 2001. His Master's research focused on AI-based computational tools to assist decision-making in the product design process. Subsequently he held a research appointment at Universidad Panamericana in Mexico City, where he worked on dynamics of parallel manipulators, and served as a consultant for the automotive industry.

Gabriel received a Ph.D. in Mechanical Engineering from Northwestern University, USA, in 2009. His doctoral project focused on impedance-based control methods for lower-limb exoskeletons. His research fields are rehabilitation robotics, physical human–robot interaction, bipedal walking and manipulator programming by demonstration.

Ambarish Goswami has been with Honda Research Institute in California, USA, for the past thirteen years, where he is currently a Principal Scientist. His field is dynamics and control, and his main research is in autonomous vehicles (leading the System Integration and Control Team), assistive exoskeletons and humanoid robots. He received the Bachelor's degree from Jadavpur University, Kolkata, India, the Master's degree from Drexel University, Philadelphia, PA, and the Ph.D. degree from Northwestern University, Evanston, IL, all in Mechanical Engineering.

Ambarish Goswami's Ph.D. work, under Prof. Michael Peshkin, was in the area of automated assembly and robot-assisted surgery. For four years following his graduation he worked at the INRIA Laboratory in Grenoble, France, as a member of the permanent scientific staff (Charge de Recherche). He became interested in human walking and in biomechanics while working on "BIP Project", the first anthropomorphic biped robot in France. This interest in gait study subsequently brought him to Prof. Norm Badler's Center for Human Modeling and Simulation at the University of Pennsylvania, Philadelphia, as an IRCS Fellow, and a three year position as a core animation software developer for 3D Studio Max at Autodesk. Ambarish has held visiting researcher positions at the Ohio State University and the University of Illinois at Urbana-Champaign for short periods. Ambarish has more than 80 publications with a total of more than 5000 Google Scholar citations; he has 14 granted patents. Ambarish serves in the Editorial Board of International Journal of Humanoid Robotics (World Scientific) and Robotica (Cambridge University Press). He is an Editor-in-Chief of the Springer Reference on Humanoid Robotics (in preparation).

Ambarish is an ASME Fellow (2013).

Please cite this article in press as: U. Nagarajan, et al., Integral admittance shaping: A unified framework for active exoskeleton control, Robotics and Autonomous Systems (2015), http://dx.doi.org/10.1016/j.robot.2015.09.015